REVISTA DE LA
ASOCIACIÓN GEOLÓGICA ARGENTINA
www.geologica.org.ar
Marzo 2026

Quaternary seismites of the Golfo San Jorge Basin, Patagonia, Argentina

Francisco Emanuel OPORTO ROMERO[1,2], José Matildo PAREDES[1], Franco Alejandro GIANNONE[1] and Matías Julián OLIVERA[1]

[1] Departamento de Geología, Facultad de Ciencias Naturales y Ciencias de la Salud, Universidad Nacional de la Patagonia "San Juan Bosco", Ruta Prov. N° 1 s/n, Km. 4, Comodoro Rivadavia, Argentina.

[2] Instituto Multidisciplinario para la Investigación y el Desarrollo Productivo y Social de la Cuenca del Golfo San Jorge (IIDEPyS-GSJ, CONICET-UNPSJB), Comodoro Rivadavia, Chubut, Argentina.

E-mail address: francisco_oporto@hotmail.com

Editor: Ricardo A. Astini

Recibido: 14/02/2026
Aceptado: 07/05/2026

ABSTRACT

This study characterizes soft-sediment deformation structures (brittle, fluid-escape, and ductile) in Quaternary deposits around Comodoro Rivadavia, Chubut, Argentina. The succession comprises a lower coastal-marine unit, a middle fluvial unit, and an upper coastal-marine unit. Deformation structures occur within stratigraphic intervals 0.6 to 3 m thick and are grouped into four deformation events: three in the lower unit and one in the upper unit. Deformation event 2 provides the most robust stratigraphic correlation between the studied localities, which are separated by ~10 km, and shows the greatest lateral continuity within the analyzed outcrops, whereas event 4 is recognized in both localities but consists of discontinuous and isolated deformation structures. Brittle structures include mesoscopic synsedimentary normal faults (n=171) with planar, rotational, or non-rotational geometries, striking from NW-SE to NE-SW (mean N349°). Reverse faults are rare (n=5). Fault planes dip on average 60°, with exposed lengths ranging from 0.78 to 134 cm and maximum vertical displacements of up to 21.4 cm. Damage zones contain secondary faults, joints, drag folds, and monoclinal folds, whereas core zones are composed primarily of claystone with minor calcium carbonate. Slickenside rake values are ~90°. Fluid-escape structures include pillars and convolute laminations, while ductile structures comprise box-folds and recumbent folds. This structural assemblage is consistent with deformation in water-saturated sediments, including liquefaction and fluidization processes. These processes may have been promoted by tidal-channel margin instability, sedimentary loading, and pore-pressure fluctuations. Event 2 is interpreted as the strongest candidate for short-lived allogenic deformation, possibly related to seismic shaking, based on its lateral persistence, correlation between distant localities, confinement within a discrete stratigraphic horizon bounded by undeformed strata, and association with synsedimentary normal faults. These results provide evidence of Quaternary deposits bearing soft-sediment deformation structures in extra-Andean Patagonia and contribute to the discussion of neotectonic activity along the north flank of the Golfo San Jorge Basin.

Keywords: soft-sediment deformation structures, autogenic and allogenic triggers, extensional tectonics, neotectonics, extra-Andean Patagonia.

RESUMEN

Sismitas cuaternarias de la Cuenca del Golfo San Jorge, Patagonia, Argentina. Este estudio caracteriza estructuras de deformación en sedimento blando (frágiles, de escape de fluidos y dúctiles) en depósitos cuaternarios alrededor de Comodoro Rivadavia, Chubut, Argentina. La sucesión comprende una sección inferior marina costera, una sección media fluvial y una sección superior marina costera. Las estructuras de deformación se desarrollan en intervalos estratigráficos de 0,6 a 3 m de espesor y se agrupan en cuatro eventos de deformación: tres en la sección inferior y uno en la sección superior. El evento 2 proporciona la correlación estratigráfica más

robusta entre las localidades estudiadas, separadas por ~10 km, y muestra la mayor continuidad lateral dentro de los afloramientos analizados, mientras que el evento 4 se reconoce en ambas localidades, pero consiste en estructuras de deformación discontinuas y aisladas. Las estructuras de deformación frágil incluyen fallas normales mesoscópicas sinsedimentarias (n=171), con geometrías planares, rotacionales o no rotacionales, y rumbos NO-SE a NE-SO (promedio N349°). Las fallas inversas son escasas (n=5). Los planos de falla presentan una inclinación promedio de 60°, con longitudes expuestas de 0,78 a 134 cm y un desplazamiento vertical máximo de 21,4 cm. Las zonas de daño contienen fallas secundarias, diaclasas, pliegues de arrastre y pliegues monoclinales, mientras que las zonas de núcleo están compuestas principalmente por arcilitas y, en menor medida, carbonato de calcio. Los valores de rake medidos en estrías son de ~90°. Las estructuras de escape de fluido incluyen pilares y laminación convoluta, mientras que las estructuras de deformación dúctil comprenden pliegues en cajón y recumbentes. Este conjunto de estructuras es compatible con deformación en sedimentos saturados en agua, incluyendo procesos de licuefacción y fluidización. Estos sucesos pudieron haber sido favorecidos por la inestabilidad de los márgenes de canales mareales, la carga sedimentaria y las fluctuaciones de la presión de poros. El evento 2 se interpreta como el candidato más robusto para registrar deformación alogénica de corta duración, posiblemente asociada a sacudidas sísmicas, debido a su continuidad lateral, correlación entre localidades distantes, confinamiento en un horizonte estratigráfico discreto limitado por estratos no deformados y presencia de fallas normales sinsedimentarias. Estos resultados aportan evidencia de deformación en sedimentos blandos en depósitos cuaternarios de la Patagonia extraandina y contribuyen a la discusión sobre la actividad neotectónica a lo largo del flanco norte de la Cuenca del Golfo San Jorge.

Palabras clave: estructuras de deformación en sedimento blando, disparadores autogénicos y alogénicos, tectónica extensional, neotectónica, Patagonia extraandina.

INTRODUCTION

Neotectonics studies recent deformations of Earth's crust, typically over the past few thousand to a few million years (Obruchev 1948, Hancock 1988, Becker 1993, Van Balen et al. 2005, Fossen 2010). The timeframe of these studies varies by region but usually spans deposits from the Late Miocene, Pliocene, or Pleistocene to the present (Bates and Jackson 1980, Delvaux and Hanon 1993). Earthquakes mainly result from the movement along plate boundaries (Hancock 1988). In areas without active plate boundaries, such as passive-margin settings, earthquakes may be associated with crustal stretching (Seth et al. 1990, Bezerra and Vita-Finzi 2000, Enzel et al. 2000, Bezerra et al. 2005, Rossetti et al. 2011).

Soft-sediment deformation structures (SSDS) form when water-saturated sediments are disrupted, often due to liquefaction and/or fluidization (Seilacher 1969, Lowe 1975, Owen 1987, Mohindra and Bagati 1996, Obermeier 1996, Montenat et al. 2007, Bezerra et al. 2005, Shanmugam 2016). Two main mechanisms can trigger SSDS: i) autogenic dynamics refer to changes within the depositional environment, including non-seismic events such as rapid sediment accumulation, debris flows, sedimentary and glacial loads, waves and storms, the migration of eolian dunes, and fluctuations of the water table (Allen 1977, Doe and Dott 1980, Postma 1983, Nataraja and Gill 1983, Rijsdijk et al. 1999, Van Vliet-Lanoë et al. 2004, Horváth et al. 2005, Le Heron and Etienne 2005, Collinson et al. 2006, Mountney 2006; Owen and Moretti 2011, Bryant et al. 2013, 2016, Pinto and Warme 2016); and ii) allogenic processes, representing phenomena external to the sedimentary system such as earthquakes (Seilacher 1969, Obermeier 1996, Owen and Moretti 2011; Buchner et al. 2020, Elías et al. 2022, Santos and Henrique-Pinto 2022). Earthquake-induced SSDS appear in sediment layers as seismites, which are deformed after deposition but before consolidation (Seilacher 1969, Mohindra and Bagati 1996, Montenat et al. 2007, Zhang et al. 2022). However, similar SSDS may result from different seismic and non-seismic triggers (Shanmugam 2016). Therefore, their interpretation as seismites requires an integrated evaluation of the deformation mechanism, sedimentological and palaeoenvironmental context, and plausible alternative triggers, rather than relying on individual deformation structures alone (Owen and Moretti 2011).

The extra-Andean Patagonia includes marine and continental lithostratigraphic units from the Late Cretaceous and Cenozoic (Fig. 1a), which are linked to second-order transgressive-regressive (T-R) cycles (Foix et al. 2025) and extensional tectonic processes (Feruglio 1930, Fossa-Mancini 1931, 1932, 1935, Leidhold 1934, Figari et al. 1999, Giacosa et al. 2004, Foix et al. 2022, Oporto Romero et al. 2023). This region also recorded compressional deformation along the San Bernardo fold belt during the Cenozoic (Encinas et al. 2018, Genge et al. 2022, Ezpeleta et al. 2024). Research has focused on seismites related to extensional tectonic events in the north flank of the Golfo San Jorge Basin (GSJB) in the Salamanca Formation (Late Cretaceous-Early Paleocene) and Río Chico Group (Early Paleocene-Middle

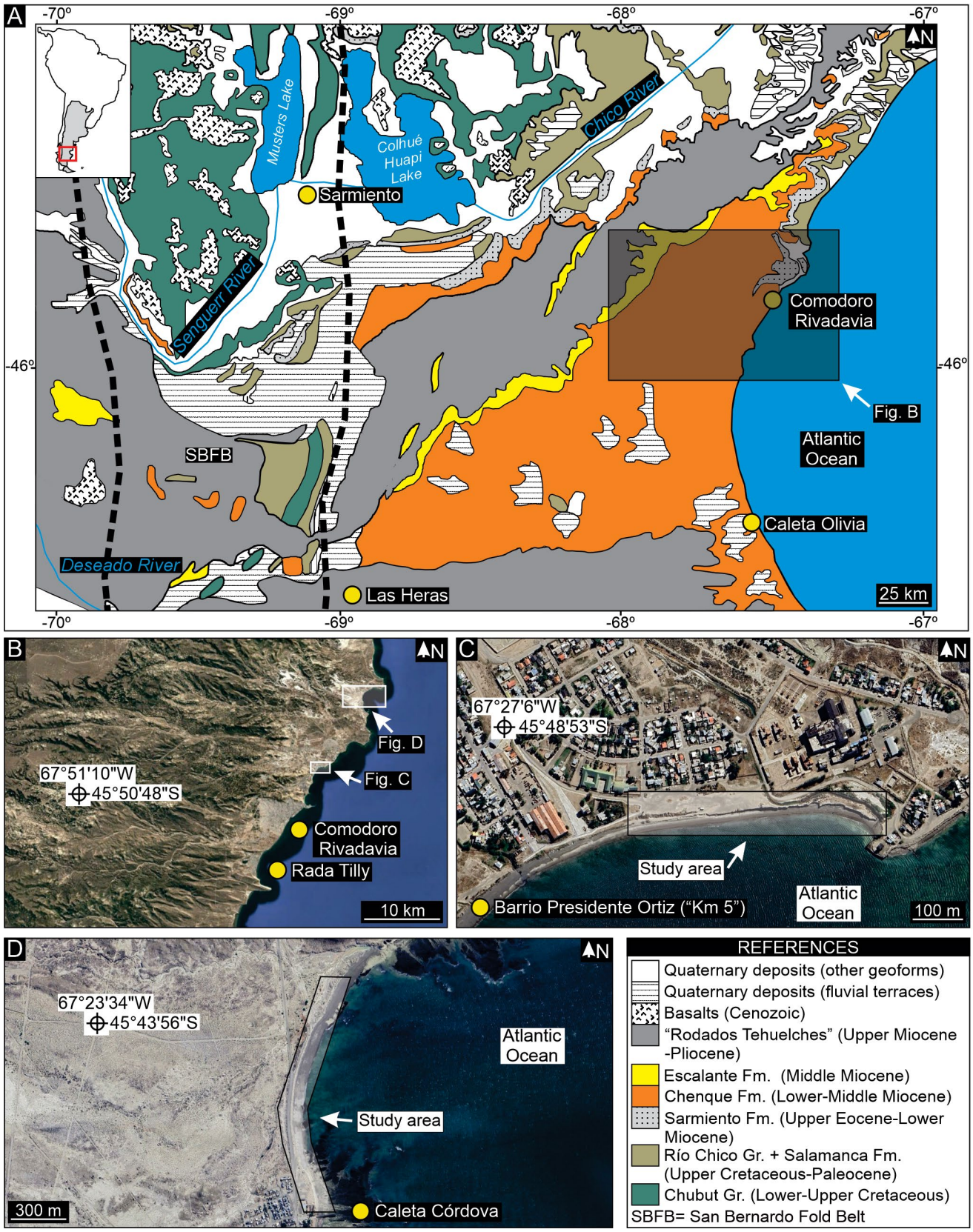

Figure 1. a) Geological map of the Golfo San Jorge Basin, after Paredes et al. (2015). The thick dashed lines mark the boundary of the San Bernardo fold belt. b) Satellite image of selected exposures analyzed in this research. c) Exposures of the Barrio Presidente Ortiz ("Km. 5"). d) Location of the study area in Caleta Córdova.

Eocene) (Foix et al. 2008), and the Middle Miocene Escalante Formation (Oporto Romero et al. 2024a). Younger rocks, such as Quaternary deposits, show exhumation and tilting due to recent crustal uplift (Codignotto et al. 1992, Rostami et al. 2000, Aguirre 2003, Schellmann and Radtke 2003, 2010, Guillaume et al. 2009, Pedoja et al. 2011). Reverse faults have been observed in Quaternary deposits along the San Bernardo fold belt (Gianni et al. 2017, Foix and Ocampo 2019, Ruiz 2024). However, Quaternary SSDS in deposits of the north flank of the GSJB have not yet been systematically documented or assessed in terms of their possible autogenic and allogenic triggers.

This study documents and analyzes SSDS in two outcrops located north of the city of Comodoro Rivadavia (Fig. 1b-d) within the north flank of the GSJB (Fig. 1a-d). The analysis focuses on documenting brittle, fluid-escape, and ductile-deformation structures preserved in Quaternary deposits. We evaluate whether some of these SSDS occur within discrete deformation horizons and may record short-lived allogenic deformation events, possibly related to seismic shaking, while also considering autogenic mechanisms inherent to the depositional system. The study asks which SSDS are present, how they are distributed stratigraphically and laterally, whether any deformation intervals can be correlated between outcrops, and which autogenic or allogenic mechanisms most plausibly explain their origin and regional significance. These findings provide constraints on the Quaternary SSDS in the GSJB and contribute to the discussion of deformation mechanisms in passive-margin settings.

GEOLOGICAL FRAMEWORK

The GSJB is an intracratonic basin in central Patagonia, between 45°-47° S and 65°-71° W (Fig. 2a). It spans about 180,000 km², with one-third of the basin now under the Atlantic Ocean (Rodríguez and Littke 2001). To the north, it borders the North Patagonian Massif and Cañadón Asfalto basin; to the south, the Deseado Region (Giacosa et al. 2010). The western margin is the Southern Patagonian Andes and the Patagonian Precordillera (Fitzgerald et al. 1990, Figari et al. 2015). Subsurface data show the eastern boundary lies on the continental margin of the Atlantic Ocean (Sylwan 2001).

The GSJB is divided into three main regions (Figari et al. 1999) based on its structural features: (1) the eastern region, comprising the north flank, basin center, and south flank; (2) the San Bernardo fold belt; and (3) the western region (Fig. 2b). The eastern region exhibits an extensional tectonic regime, as indicated by normal faults striking W-E, SE-NW, and SW-NE (Fig. 2c). The north flank contains normal faults with steeper dip angles than those of the south flank, and the thickest depocenters are found in the basin center. In both the north flank and basin center, most normal faults dip toward the SW, whereas in the south flank, most faults dip toward the NE. The San Bernardo fold belt is characterized by NNW-SSE-trending mountain ranges resulting from compressional uplift since the late Cretaceous (Allard et al. 2025). The western region, situated immediately west of the San Bernardo fold belt, contains Cretaceous depocenters associated with extensional tectonics, and also exhibits a mild positive tectonic inversion (Figari et al. 1996, Navarrete et al. 2015).

The uppermost Jurassic and Cretaceous sedimentation of the GSJB took place in an endorheic basin, whose evolution has been the subject of intense research for up to a century, largely due to the importance of hydrocarbon accumulations in the subsurface and outcrop analogs along the San Bernardo fold belt (see Paredes et al. 2021).

Progressing into the uppermost Cretaceous to Cenozoic, the eastern region of the GSJB evolved to a passive-margin setting characterized by low tectonic subsidence (Legarreta et al. 1990, Legarreta and Uliana 1994, Malumián et al. 1999). This shift in setting led to the development of three second-order transgressive-regressive cycles, represented by an integrated sedimentary succession up to ~1,500 m thick, spanning the Upper Cretaceous to Pliocene deposits (Fig. 3), and coeval with several extensional tectonic events (Foix et al. 2025). The first of these second-order transgressive-regressive cycles, spanning the Upper Cretaceous to Upper Eocene, comprises the Salamanca Formation (shallow marine to shelf environment), the Río Chico Group (fluvial), and the lower section of the Sarmiento Formation (pyroclastic-rich loess) (Fig. 3), with a total thickness of about 600 m (Feruglio 1949, Sciutto et al. 2000, 2008, Raigemborn et al. 2010, Foix et al. 2025). The second cycle (Upper Eocene-Lower Miocene) includes the El Huemul Formation (shallow marine) and the upper units of the Sarmiento Formation (continental pyroclastics) (Fig. 3), reaching a thickness of about 200 m (Paredes et al. 2015, Foix et al. 2025). Finally, the third cycle (Lower-Middle Miocene) is represented by the Chenque Formation (shallow marine to shelf environment) and the Escalante Formation (fluvial-eolian) (Fig. 3), with an integrated thickness of approximately 710 m (Feruglio 1949, Bellosi 1995, Sciutto et al. 2000, 2008, Cuitiño et al. 2015, Oporto Romero and Paredes 2022, Oporto Romero et al. 2024b, Foix et al. 2025). The younger units include gravel sheets of Upper Miocene-Pliocene age, referred to as “Rodados Tehuelches” (fluvial) and reworked deposits in paleotopographic lowlands

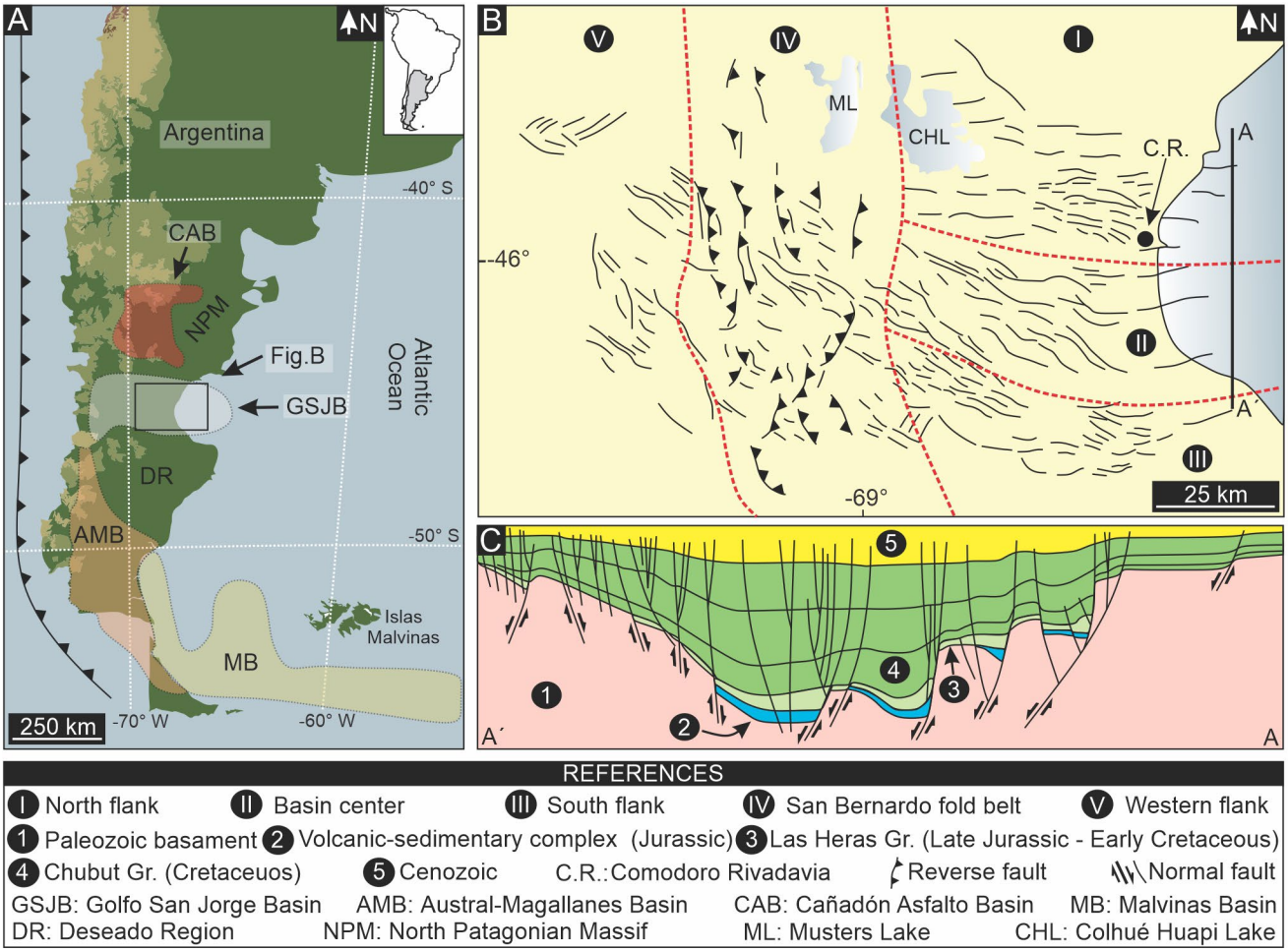

Figure 2. a) Location map of the GSJB. b) Structural regions of the GSJB. This information was sourced from Ramos (2015). c) N-S seismic section (A-A') showing the subsurface basin and the distribution of the main units of the eastern region. Modified from Figari et al. (1999).

and river valleys associated with the post-Miocene uplift of the GSJB (Martínez and Kutschker 2011, Bilmes et al. 2021).

During the Quaternary, minor transgressive-regressive cycles were recorded in low-relief coastal areas of the GSJB (Rostami et al. 2000, Sciutto et al. 2000, 2008, Montes et al. 2015, Desiage et al. 2023). Specifically, the Pleistocene-Holocene record is characterized by late Pleistocene-Holocene coastal ridges overlain by Holocene fluvial, eolian, ephemeral-lakes, and shallow marine sediments (Feruglio 1949, Codignotto et al. 1992, Schellmann and Radtke 1997, 2000, 2003, 2010, Aguirre 2003, Pedoja et al. 2011, Montes et al. 2015, Rodríguez et al. 2025). In addition, the offshore subsurface stratigraphy of the San Jorge Gulf, based on high-resolution seismic profiles and sediment cores, reveals successions of estuarine environments resulting from a marine transgression of late Pleistocene to middle Holocene age, which inundated a paleo-fluvial network (Desiage et al. 2023). Although these offshore deposits are not necessarily time-equivalent to the outcropping deposits analyzed in this study, they provide a useful regional comparison in terms of depositional setting. The studied outcrops are broadly constrained to the Quaternary, but they lack absolute ages that would allow a direct chronostratigraphic correlation with the late Pleistocene–middle Holocene offshore record. Thus, the comparison is restricted to sedimentological and paleoenvironmental similarities, particularly the development of estuarine to coastal-marine depositional systems, rather than temporal equivalence.

Finally, extra-Andean Patagonia underwent tectonic uplift during the Quaternary, as evidenced by the exhumation, tilting, and stepped arrangement of fluvial and coastal marine terraces (Codignotto et al. 1992, Rostami et al. 2000, Pedoja et al. 2011, Guillaume et al. 2013, Ávila and Dávila 2020). At present, neotectonic activity in extra-Andean Patagonia has been attributed to dynamic topography related to slab window processes (Pedoja et al. 2011, Guillaume et al. 2013) and slab tearing (Navarrete 2025).

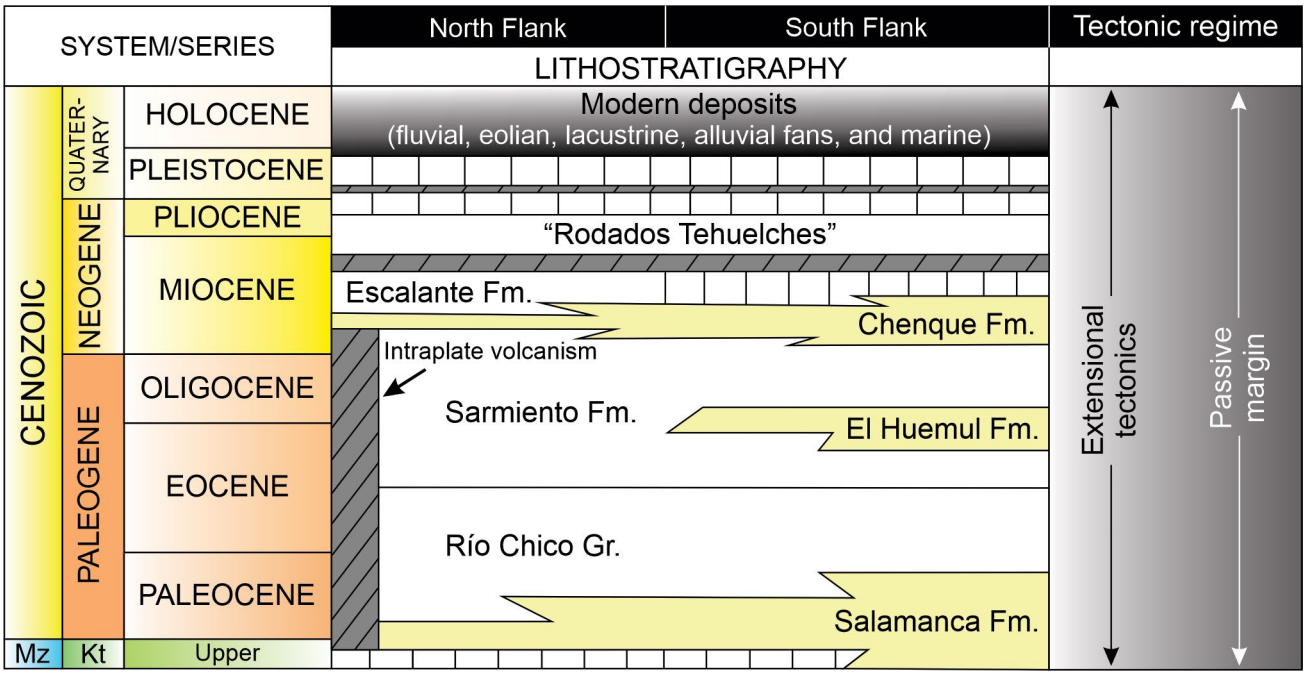

Figure 3. Upper Cretaceous-Cenozoic stratigraphy of the eastern region of the GSJB and its tectonic regimes based on Plazibat et al. (2019). The yellow units are of marine origin, the white units indicate continental environments, and the gray units are basic volcanic successions. Vertical lines indicate hiatus. The shaded interval marks the Quaternary deposits analyzed in this study.

METHODOLOGY

The fieldwork involved the description and interpretation of SSDS in Quaternary deposits on the north flank of the GSJB. The suite of structures was classified according to their morphology, genesis, or spatial dimension (Montenat et al. 2007, Moretti and Sabato 2007, Üner 2014). SSDS were categorized based on formation processes as brittle deformation, fluid-escape, and ductile deformation structures, and analyzed for orientation, architecture, and topology within each category (Owen 1987, 2003, Fossen 2010, Elías et al. 2022). The fault analysis was based on the size of the core zone and mineral filling, the extent of the damage zone and associated structures, strike, dip, dip direction, geometry, kinematics, and preservation of slickensides on the slip surface. Spatial data on mesoscopic faults (strike, dip, and dip direction) were represented using Stereonet 11 and GEOrient software to generate stereographic projection graphs (equiareal, lower hemisphere), rose diagrams, poles, and polar density graphs. In fluid-escape and ductile deformation structures, we obtained data on the orientation of deformed laminations, geometry of the structures and infill types, and the orientation of axial planes in folds.

RESULTS

Stratigraphic framework of the studied succession

Quaternary deposits outcrop along the coast between Comodoro Rivadavia - Presidente Ortiz and Caleta Córdova (Figs. 1b-c and 3). In the studied localities, the succession is 12.9-13.5 m thick and can be divided into three units based on sedimentary environments and lithofacies associations recognized in the measured sections (Fig. 4).

The lower unit is 7.5 to 3.9 m thick and corresponds to a coastal-marine interval composed of mud-dominated tidal-bar deposits (Fig. 5a), tidal-flat facies associations (Fig. 5b-c), and tidal channel-fill deposits (Fig. 5b). This unit is mainly characterized by heterolithic, rhythmically laminated, fine-grained beds with mud drapes, root traces, and locally organic-rich intervals, consistent with tidal-flat to marginal coastal settings. The middle unit is 3.9 to 1.9 m thick and is interpreted as fluvial. It consists of paleosol horizons interbedded with proximal floodplain facies associations, including crevasse-splay and crevasse-channel deposits (Fig. 5c-d). This unit records alternation between subaerial exposure, pedogenic modification, and episodic sedimentation in floodplain settings. No SSDS were recognized in this middle fluvial unit; therefore, it is not considered part of the deformed intervals

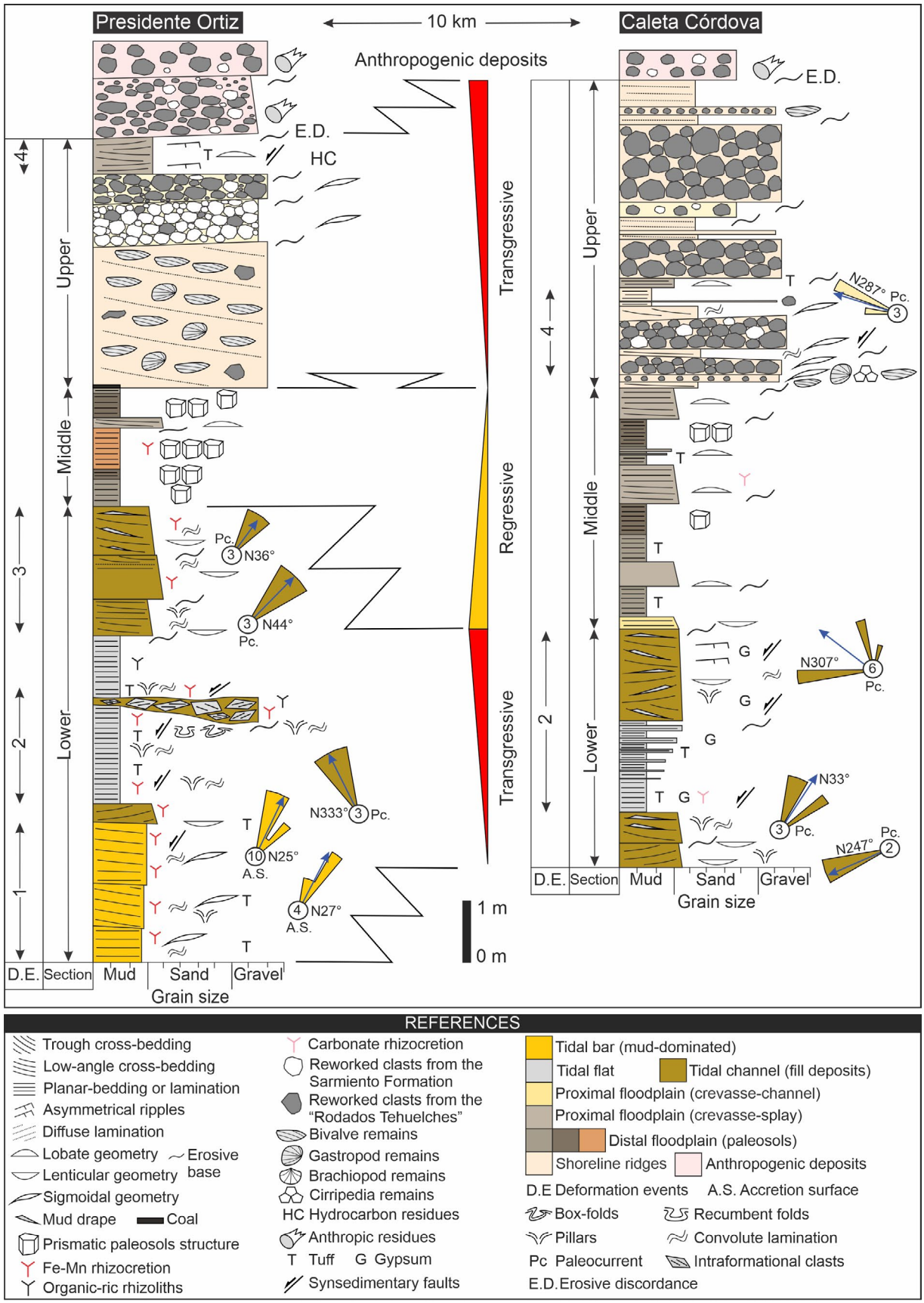

Figure 4. Sedimentological profiles of the Quaternary succession at Presidente Ortiz and Caleta Córdova, showing lithofacies associations, transgressive–regressive trends, deformation events, and SSDS distribution within the lower and upper coastal-marine units.

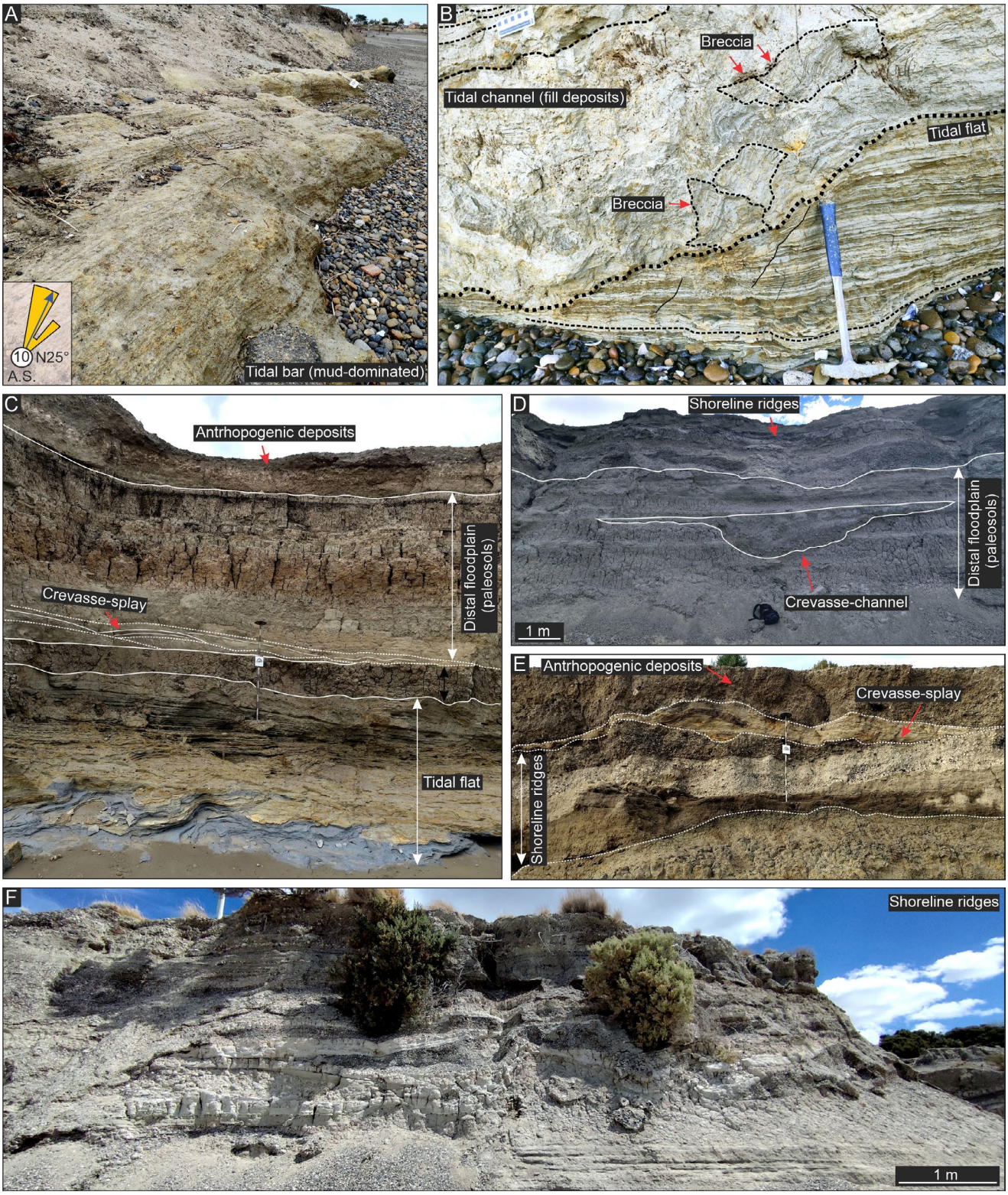

Figure 5. Representative outcrops and lithofacies associations of the studied Quaternary succession. a) Mud-dominated tidal bar facies association of the lower coastal-marine unit. b) Tidal channel (fill deposits) facies association of the lower coastal-marine unit, showing intraformational breccias and their relationship with adjacent tidal flat deposits. c) Contact between the tidal flat facies association of the lower coastal-marine unit and the distal floodplain (paleosols) and crevasse-splay facies associations of the middle fluvial unit. d) Distal floodplain (paleosols) and crevasse-channel facies associations of the middle fluvial unit, overlain by shoreline ridge deposits of the upper coastal-marine unit. e) Shoreline ridge and associated crevasse-splay facies associations of the upper coastal-marine unit. f) General view of the shoreline ridge facies association of the upper coastal-marine unit. The hammer is 42 cm long, and Jacob's staff is 1.5 m long.

analyzed below. The upper unit is 5.0 to 4.1 m thick and consists of coastal-marine deposits represented by shoreline-ridge and associated crevasse-splay facies associations (Fig. 5d-f). These deposits include sandy to gravelly beds and represent the uppermost depositional interval of the analyzed succession. The vertical stacking of a lower coastal-marine unit, a middle fluvial unit, and an upper coastal-marine unit provides the stratigraphic framework for evaluating SSDS distribution across the studied profiles.

Centimeter- to meter-scale SSDS were identified within this stratigraphic framework and incorporated into high-resolution sedimentological profiles to evaluate their vertical distribution, lateral continuity, and stratigraphic recurrence (Fig. 4). The documented structures include brittle deformation, fluid-escape, and ductile deformation structures. They are organized into four deformation events or intervals, although their stratigraphic expression and lateral continuity differ among events. Event 1 is restricted to Presidente Ortiz, where it is 2.3 m thick and laterally continuous for up to 30.6 m. Event 2 occurs in both Presidente Ortiz and Caleta Córdova, with thicknesses of 1.9 m and 3.0 m and lateral continuities of 489 m and 1086 m, respectively; this event contains the highest abundance and diversity of SSDS. Event 3 is only exposed at Presidente Ortiz, where it reaches 2.1 m in thickness and can be traced laterally for 489 m. Event 4 is recognized in both Presidente Ortiz and Caleta Córdova, affecting intervals of 0.6 m and 1.4 m thick, respectively. However, unlike events 2 and 3, it does not form a tabular deformation horizon with laterally continuous SSDS bounded by undeformed strata. Instead, deformation structures occur as isolated features within the upper coastal-marine deposits. Events 1, 2, and 3 display tabular geometries and are sharply bounded by undeformed deposits, supporting their recognition as discrete stratigraphic deformation intervals. Deformation events were evaluated between localities based on stratigraphic position, sedimentary environment, facies associations, topographic elevation, thickness, and lateral continuity. Based on these criteria, event 2 shows the most robust stratigraphic and lateral correlation between Presidente Ortiz and Caleta Córdova, two localities separated by ~10 km (Fig. 1b-d). Event 4 is also recognized in both localities (Fig. 4), but it does not define a continuous tabular deformation horizon and is therefore treated as a discontinuous interval of isolated deformation structures rather than as a laterally correlatable deformation horizon. Events 1 and 3 are restricted to Presidente Ortiz and were not identified at Caleta Córdova. The most abundant and diverse SSDS occur in Presidente Ortiz, whereas Caleta Córdova records fewer brittle deformation structures and subordinate fluid-escape structures. Therefore, the strongest stratigraphic argument for event correlation is provided by event 2, whereas event 4 is considered only as a discontinuous deformation interval recognized in both localities.

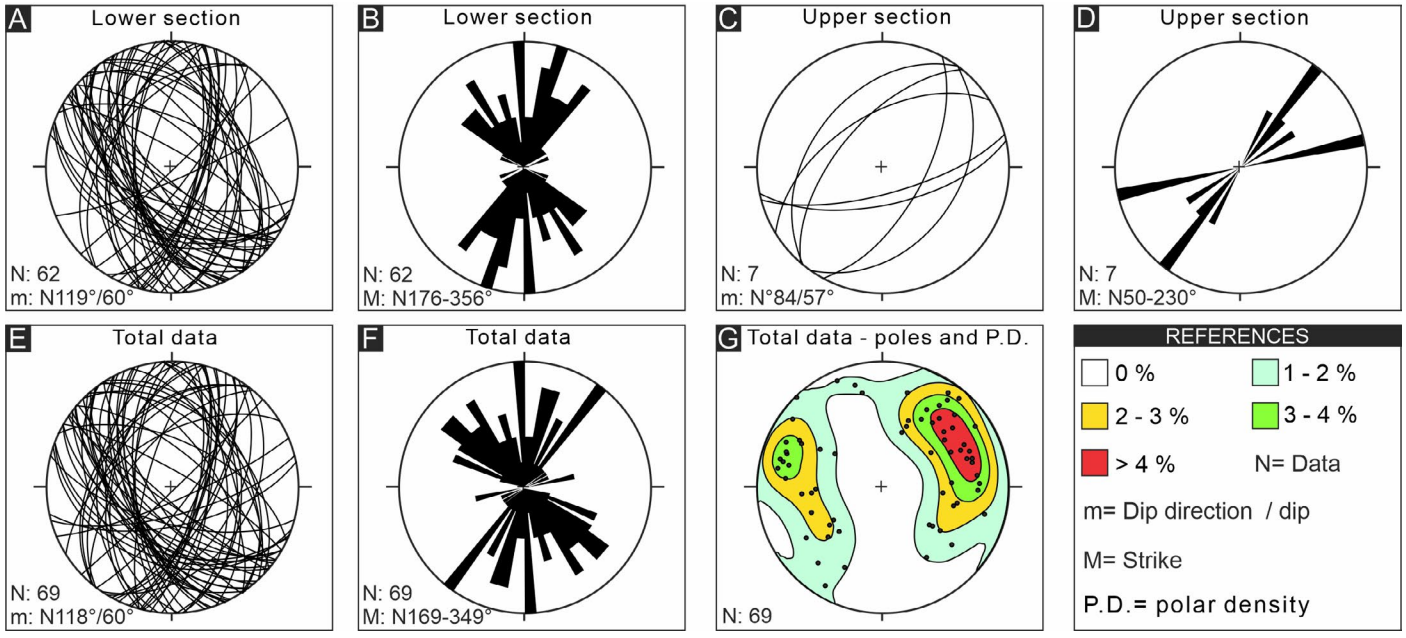

Figure 6. Representation of normal mesoscopic faults for each section in stereographic projections (equiareal, lower hemisphere) and rose diagrams. a) Stereographic projection of the lower section. b) Rose diagram of the lower section. c) Stereographic projection of the upper section. d) Rose diagram of the upper section. e) Stereographic projection of all data. f) Rose diagram of all data. g) Stereographic projection of poles and polar density diagram for all data.

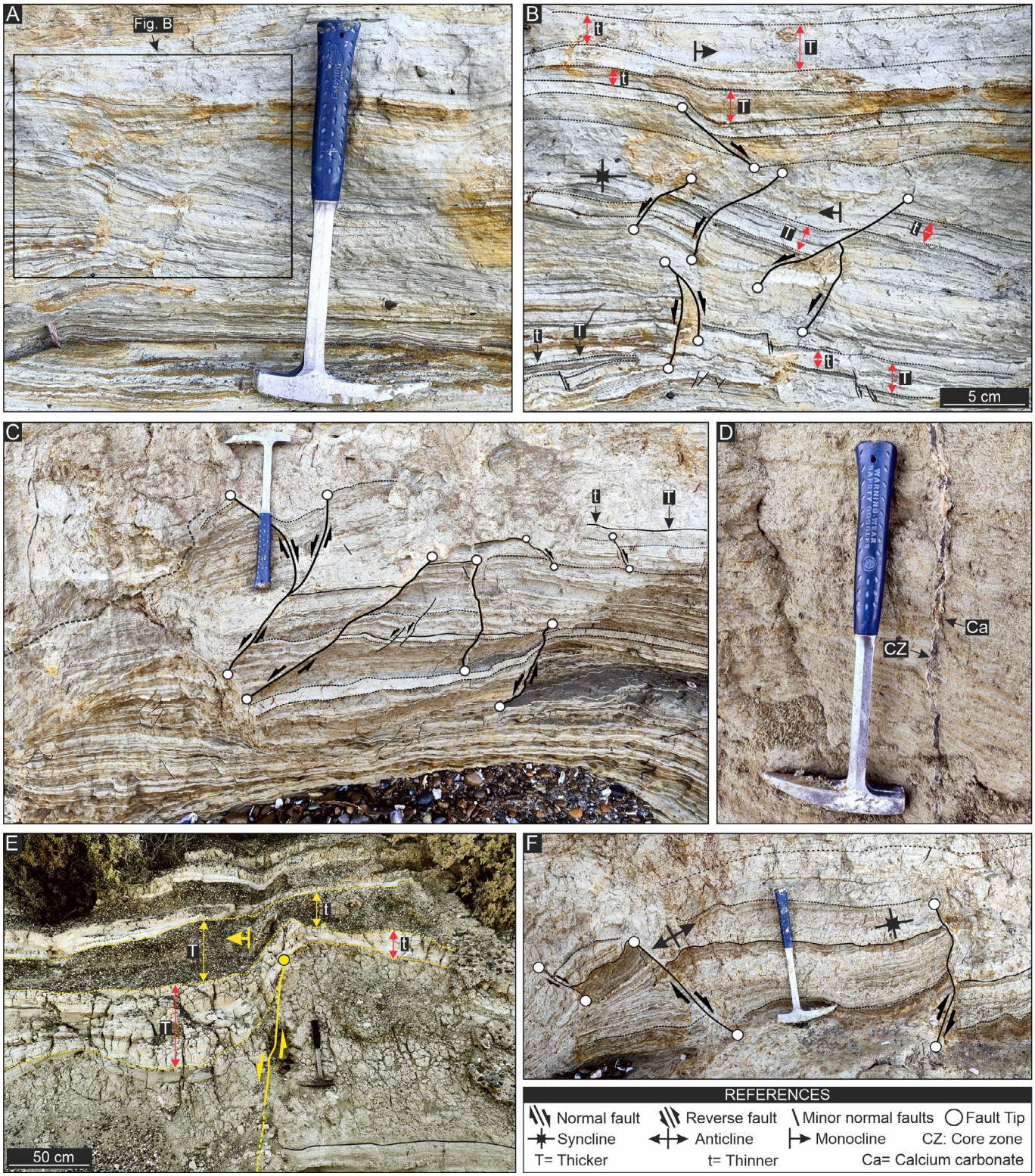

Figure 7. Brittle deformation structures: faults and associated structures. a) Claystones of the tidal flat deposits (lower section) affected by mesoscopic normal faults (uninterpreted). b) Close-up and interpretation of planar, rotational, and non-rotational mesoscopic normal faults. Note the monoclinal folds, anticlinal drag, and thickness differences between the hanging-wall and foot-wall fault blocks. c) Tidal flat deposits (lower section) affected by non-rotational, planar mesoscopic normal faults. Observe thickness changes between the hanging-wall and foot-wall fault blocks. d) Sub-vertical fault surface with calcium carbonate (Ca) in the core zone (CZ), developed in the lower section. e) Mesoscopic normal fault developed in shoreline ridges (upper section). Notice the thickness variation between fault blocks and the development of monocline folds due to vertical fault-propagation. f) Mesoscopic faults with normal and reverse kinematics in tidal flat deposits (lower section). Observe the anticlinal and synclinal drag. The hammer measures 42 cm long.

Soft-sediment deformation structures

Brittle deformation structures

We identified 176 mesoscopic faults, of which 171 have normal kinematics (97.2%), and 5 display reverse kinematics (2.8%). We obtained strike, dip direction, dip, and slickensides measurements from 69 normal faults and 2 reverse faults, as many exposed fault planes (59.7%) are only preserved at the millimeter to centimeter-scale, which preclude the acquisition of directional data. Mesoscopic normal faults occur mainly in tidal bar (mud-dominated), tidal flat, and tidal channel (fill deposits) of tuffaceous and siliciclastic composition in the lower coastal-marine unit (Figs. 6a-b and 7a-b), and subordinately within crevasse-splay and shoreline-ridge deposits of the upper coastal-marine unit (Figs. 6d-e and 7e). These structures were documented in the first, second, and fourth deformation events (Fig. 4). In contrast, the reverse faults are restricted to the second deformed interval, affecting tidal flat deposits (Fig. 4). In summary, 169 faults (96.0%) were identified in the lower coastal-marine unit, and seven faults (4.0%) occur in the upper coastal-marine unit.

Synsedimentary faults and associated structures

Fault surfaces: The structures have rotational planar geometry (Fig. 7a,b) or non-rotational geometry (Fig. 7a-f) and are planar along their length with dip changes where silt or sand-sized lithologies alternate with clay-rich strata (Fig. 7a-c and f). The exposed lengths of the fault planes range from 0.78 to 134 cm, with dip angles between 38° and 88° (average: 60°; Fig. 6e-f). The normal faults have strike orientations ranging between NW-SE and NE-SW (Fig. 6a-f), with an average strike of N 349° (Fig. 6f) and an average dip direction of N 118° (Fig. 6e and g). The total data set records two main subpopulations of mesoscopic faults (two families of conjugate faults), evidencing wide dispersion of strike (Fig. 6a-g). Additionally, subpopulations of secondary faults (1 or 2 families of conjugate faults) are oriented obliquely or transversely to the main subpopulations (Fig. 6e-f). It is common for secondary normal faults to be rooted in a higher-level structure (Fig. 7a-c). The poles of the faults and polar density data (Fig. 6g) indicate clustering in the distribution. Normal faults show thickness increase in the hanging-wall block (Fig. 7a-c and e) and commonly display wedge geometries (Fig. 7a-b and e). The expansion index values (Thorsen 1963) range from 1.08 to 2.85 and occur in strata less than 53 cm thick. The five mesoscopic reverse faults occur adjacent to and subparallel to mesoscopic normal faults (Fig. 7f).

Damage and core zones: Structures of higher hierarchy show damage zones with lateral continuity < 1 m, which are associated with tip and wall damage zones (Kim et al. 2004). Within these damage zones, minor faults as well as parallel, conjugate, and oblique joints are present both laterally and vertically relative to the larger structures, typically spaced by centimeters (Fig. 7a-c). Half-graben geometries frequently develop in these settings (Fig. 7a-b and c). The damage zones show anticlinal and monoclinal folds associated with normal drag, which terminate at the fault plane (Fig. 7a-b and f). Mesoscopic faults are characterized by small-scale displacements, reaching up to 21.4 cm. Core zones generally exhibit a simple configuration (Fig. 7a-f) consisting of a single plane that accommodates deformation (Faulkner et al. 2010) but may also contain gray and white clays and, occasionally, calcium carbonate precipitation (Fig. 7d), with thicknesses ranging from 1 to 2-3 mm. The rake values of slickensides on fault surfaces are approximately 90°.

Interpretation: Faults that display increased thickness in the hanging-wall block compared to the preserved thickness in the foot-wall block are indicative of synsedimentary fault growth and deformation coeval with sedimentation (Childs et al. 2017). Although thickness variations may be slightly modified by compaction or erosion, they reflect distinct stages of individual fault development (Childs et al. 2003). Rake values of 90° on slickensides indicate faults with predominant dip displacement. Vertical variation in the fault surface angles is associated with differences in the strength of deformed lithologies (Foix et al. 2012). Drag folds and secondary faults are produced by friction between strata along the fault surface (Japas et al. 2008), whereas monocline folds result from the propagation of the deformation away from the fault tip (Conneally et al. 2017). The formation of folds and faults is attributed to the interplay of continuous and discontinuous deformation events (Childs et al. 2017). The low to zero lithostatic pressure of the unconsolidated material at the surface favors the simultaneous development of normal and reverse faults during the same deformation event (Fossen 2010).

Fluid-escape structures

Fluid-escape structures are recorded in the first three deformation events of the lower section, within tidal bar (mud-dominated), tidal channel and tidal flat facies (Fig. 4). In particular, fluid-escape structures are especially abundant in the Presidente Ortiz locality and subordinate in Caleta Córdova exposures, where they consist of pillars and convolute lamination. The following sections describe these structures in more detail.

Pillars

Description: Clay-rich deposits that make up the tidal bar (mud-dominated) (event 1), tidal flat and tidal channel deposits (event 2), and tidal channel sandstones (event 3) in Presidente Ortiz locality exhibit vertical, V-shaped deformation structures (Fig. 4). These structures cut through the primary sedimentary structures, with downward deflections (Fig. 8a), forming pillars. Their maximum vertical dimension reaches 1.09 m, with depressions filled by interbedded layers of claystone and siltstone (Fig. 8a). Pillars occur in strata of high lateral continuity, and they can be organized laterally or vertically (Fig. 8a).

Interpretation: Fine lithologies with deformation structures serve as impermeable or semi-permeable barriers that increase pore pressure (Lowe and LoPiccolo 1974, Postma 1983, Obermeier 1996). In water-saturated sediments, fluidization processes respond to pressure gradients and promote the development of fluid-escape structures (Owen 2003, Bezerra et al. 2005). These short-lived events allow solid granular material to behave like a liquid (Allen 1982). When material moves vertically, fluidization forms pillars in the sediments (Kunii and Levenspiel 1969, Pinto and Warme 2016, Lowe 1975). Such structures are comparable to “pipes”, “type B pillars”, or “elutriation columns” (see Foix et al. 2008).

Convolute lamination

Description: Tuffaceous and siliciclastic clays of the tidal bars (mud-dominated) (event 1), tidal flat (event 2), sandstones of the tidal channels (event 3), and shoreline ridges (event 4) exhibit convolute lamination (Fig. 4). Characterized by folded and contorted laminations within a stratum (Fig. 8b), these deformation structures achieve a maximum thickness of 33.9 cm and have lateral continuity on a metric scale. Although recognized in both analyzed exposures, they remain subordinate in Caleta Córdova.

Interpretation: Liquefaction and fluid-escape processes result from pressure gradients and increased pore pressure in water-saturated sedimentary material (Seed and Idriss 1971, Owen 2003, Bezerra et al. 2005). During liquefaction or fluidization, the sediment framework temporarily loses strength and may behave as a liquid-like material (Lowe 1975, Allen 1982). Convolute lamination is equivalent to convolute stratification or contorted lamination/stratification (Allen 1977, Collinson et al. 2006).

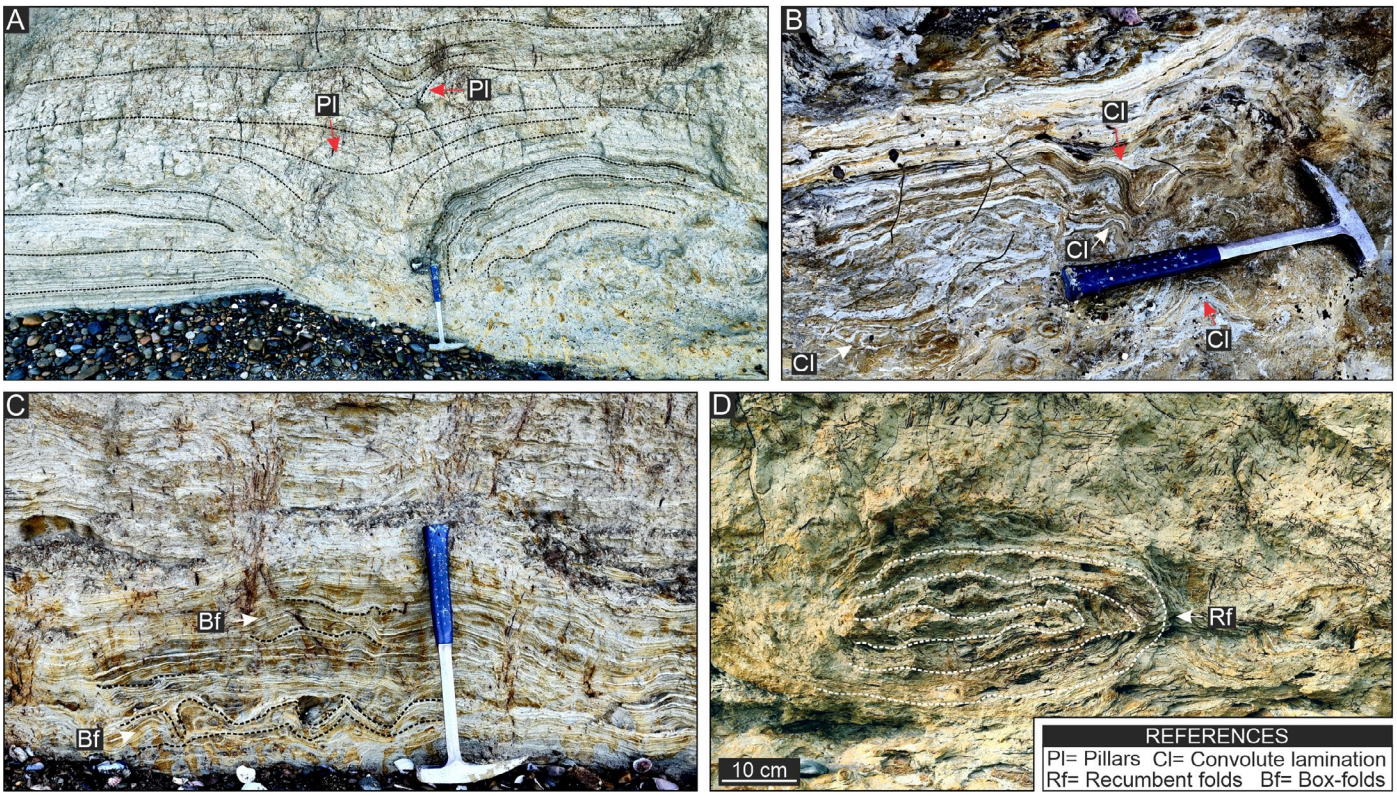

Figure 8. Fluid-escape structures and ductile deformation structures in tidal flat deposits. a) Pillars, observe the V-shape and deformation of the lamination. b) Convolute lamination adjacent to normal and reverse mesoscopic faults. c) Centimeter-scale box folds (Bf). d) Recumbent fold, with deformed laminations. The hammer is 42 cm long, and the pen measures 14.9 cm.

Ductile deformation structures

Ductile deformation structures occur in the Presidente Ortiz locality, in fine-grained deposits (mostly tuffaceous-siliciclastic deposits) representing tidal flat environments (Fig. 4). The suite of ductile deformation features includes box- and recumbent folds.

Folds

Description: Box-folds are present in claystones and siltstones, both tuffaceous and siliciclastic, within tidal flat deposits affected by the second deformation event. These structures display anticlinal and synclinal folds with multiple axial planes oriented randomly (Fig. 8c). The maximum thickness of box-folds is 9.4 cm, and their lateral continuity ranges from centimeters to meters. Recumbent folds are also observed in claystones and siliciclastic siltstones of the tidal flat (Figs. 4 and 8d). These consist of anticlines and synclines with subhorizontal axial planes and hinge lines (Fig. 8d), with a maximum thickness of 31.4 cm and exhibiting centimetric lateral continuity.

Interpretation: Recumbent folds and box-folds in claystones and siltstones are interpreted as resulting from granular flows triggered by a reduction in effective confining pressure and an increase in pore-fluid pressure (Twiss and Moores 1992). These processes induce a temporary change in the rheological state, transitioning from a solid to a liquefied state (Owen 2003). Such conditions facilitate the formation of folds that accommodate the deformation within the stratum (Allen and Banks 1972, Allen 1982). According to Elías et al. (2022), the box-folds are comparable to those described as “seismoslumps” or “slump-like structures” (Montenat et al. 2007, Moretti and Sabato 2007).

DISCUSSION

Origin of soft-sediment deformation structures

SSDS develop when unconsolidated to poorly consolidated, commonly water-saturated sediments are deformed before final lithification or consolidation (Seilacher 1969, Mohindra and Bagati 1996, Montenat et al. 2007). Their origin may involve autogenic mechanisms related to local depositional processes and early post-depositional changes, as well as allogenic triggers external to the depositional environment (Montenat et al. 2007, Owen and Moretti 2011, Shanmugam 2016). Autogenic or non-seismic processes include: (i) waves and storms (Nataraja and Gill 1983, Owen 1987, Owen and Moretti 2011), (ii) cryogenic/thermokarst disturbances and subglacial hydrofracturing (Van Vliet-Lanoë et al. 2004, Le Heron and Etienne 2005, Pinto and Warme 2016), (iii) debris flows and alluvial fans (Lowe 1975, Postma 1983), (iv) migration of eolian dunes and granular flows (Doe and Dott 1980, Mountney 2006), (v) rapid sediment accumulation and/or sedimentary loading (Allen 1977, Horváth et al. 2005, Collinson et al. 2006), and (vi) fluctuations in the water-table level through time (Bryant et al. 2013, 2016). In contrast, allogenic triggers, particularly seismic shaking, may generate comparable deformation structures in water-saturated sediments through liquefaction, fluidization, or brittle deformation (Obermeier 1996, Owen and Moretti 2011, Buchner et al. 2020, Zhang et al. 2022). Therefore, the interpretation of SSDS as seismites requires an integrated assessment of possible seismic and non-seismic triggers, including the sedimentological context, deformation mechanism, stratigraphic distribution, lateral continuity, recurrence of deformed horizons, and association with synsedimentary structures, rather than relying on the morphology of individual structures alone.

The deformed deposits analyzed in this study are part of a coastal-marine system, including tidal-flat, mud-dominated tidal-bar, and tidal channel-fill deposits (lower section), and shoreline ridges and crevasse-splays (upper section) (Fig. 4). The middle fluvial unit does not contain recognized SSDS and is therefore not considered part of the deformed intervals discussed here. In the lower coastal-marine unit, the rhythmic heterolithic lamination of tidal-flat deposits, together with adjacent tidal channel-fill deposits, indicates a setting in which local autogenic deformation could have been promoted by tidal-current reworking, lateral erosion of cohesive channel margins, bank collapse, local slumping, intraformational brecciation, sedimentary loading, and changes in pore-water pressure (Ginsberg and Perillo 1990, Scasso et al. 2012). In the upper coastal-marine unit, shoreline-ridge and associated crevasse-splay deposits may have been affected by high-energy coastal processes, density flows, rapid sediment accumulation, and local loading. Wave- or storm-related processes could have contributed to local reworking in this upper unit, but the available facies evidence does not allow them to be identified as the main trigger of the documented deformation. Cryogenic or thermokarst processes, subglacial hydrofracturing, alluvial-fan deposition, and eolian-dune migration are not supported by the observed facies associations. Likewise, although water saturation was likely common in these coastal-marine settings, independent evidence for deformation driven specifically by groundwater-table fluctuations is not available. Therefore, autogenic processes are considered plausible local mechanisms within the coastal-marine units, particularly where deformation is spatially restricted or associated with tidal-channel

margin instability, density-flow processes, rapid sediment accumulation, or local loading. However, these mechanisms cannot be generalized as a single explanation for all deformed intervals, especially where deformation is laterally persistent and associated with synsedimentary normal faults (Fig. 7).

SSDS recognized in the studied succession display several characteristics that may be linked to short-lived allogenic triggers, including seismic shaking related to extensional tectonic activity. These characteristics include: (i) lateral continuity from tens to hundreds of meters per outcrop, locally exceeding 1 km in event 2; (ii) correlation of event 2 between Presidente Ortiz and Caleta Córdova, two localities separated by ~10 km (Figs. 1b-d and 4); (iii) confinement of deformation within thin, discrete stratigraphic horizons, 0.6–3.0 m thick, bounded below and above by undeformed strata (Fig. 4); and (iv) the occurrence of mesoscopic synsedimentary normal faults characterized by thickness increases in the hanging-wall block (Fig. 7a-c, e). However, these criteria are not equally developed in all deformation events, and local autogenic processes may have contributed to some structures. Therefore, each event is evaluated separately according to its facies association, type of SSDS, lateral continuity, stratigraphic position, and association with synsedimentary normal faults.

Event 1 is restricted to Presidente Ortiz, where the outcrop is erosionally limited and lacks extensive lateral continuity. In its preserved portion, the event is 2.3 m thick and can be traced laterally for 30.6 m. Its limited preservation prevents a robust assessment of its original lateral extent and regional significance. However, the presence of synsedimentary normal faults leaves open the possibility of an allogenic contribution, although local autogenic processes cannot be ruled out. Event 2 is recorded at both Presidente Ortiz and Caleta Córdova, where it is 1.9 m and 3.0 m thick, respectively, and laterally continuous for up to 489 m and 1086 m. This event contains the highest abundance and diversity of SSDS, including brittle, fluid-escape, and ductile deformation structures. Although local autogenic processes related to tidal-flat deformation, sedimentary loading, pore-pressure changes, or tidal-channel margin instability may have contributed to some structures, the lateral continuity, correlation over ~10 km, confinement within a discrete stratigraphic horizon bounded by undeformed strata, and abundance of synsedimentary normal faults support an allogenic trigger, most plausibly seismic shaking. Event 3 is exposed only at Presidente Ortiz, where it is 2.1 m thick and can be traced laterally for 489 m. Unlike event 2, it lacks synsedimentary normal faults; therefore, its origin may be more readily explained by autogenic processes related to tidal-channel dynamics, channel-margin collapse, sedimentary loading, or local pore-pressure changes. However, given its lateral continuity and position within the deformed succession, an allogenic contribution cannot be completely excluded. Event 4 is recognized at both Presidente Ortiz and Caleta Córdova, where it is 0.6 m and 1.4 m thick, respectively. However, unlike event 2, the deformed horizons and synsedimentary normal faults are discontinuous and cannot be traced laterally as a continuous deformation horizon between outcrops. This event is mainly represented by isolated mesoscopic synsedimentary normal faults, locally associated with subordinate convolute lamination in crevasse-splay facies. Therefore, event 4 is not interpreted here as a seismite sensu stricto. The isolated convolute lamination may have formed through local liquefaction related to rapid sediment accumulation and/or sedimentary loading, whereas the occurrence of synsedimentary normal faults indicates brittle deformation compatible with extensional tectonic activity. Thus, event 4 is better interpreted as a mixed interval in which local autogenic processes affected some facies, while synsedimentary normal faulting records a tectonic component.

The structures described here have close analogues in passive-margin basins affected by seismic shaking. In Quaternary deposits of northeast Brazil, liquefaction-induced fluid-escape structures comparable to pillars were interpreted as paleoseismic features (Bezerra et al. 2005). In the São Luís Basin, northern Brazil, convolute lamination and recumbent folds were related to paleoseismicity in a passive-margin setting (Rossetti 1999). In the Douala sub-basin, Cameroon margin, box-folds and recumbent folds were interpreted as SSDS associated with seismic shocks (Djomeni et al. 2011). However, in the GSJB, the strongest argument for a possible seismic trigger is not the presence of fluid-escape and ductile deformation structures alone, but their association with synsedimentary normal faults, discrete deformation horizons, and lateral correlation between outcrops, especially in event 2.

Neotectonics of the Golfo San Jorge Basin

Along the Patagonian coast, between Puerto Deseado and Bahía Bustamante, there are stepped marine terraces from the late Pleistocene-Holocene associated with Quaternary tectonic uplift events (Codignotto et al. 1992, Rostami et al. 2000, Aguirre 2003, Schellmann and Radtke 2003, 2010, Pedoja et al. 2011, among others). In addition, tilted fluvial terraces have been identified in the Senguerr River and Deseado River (see Fig. 1a), and have been uplifted by neotectonic events (Guillaume et al. 2009, Pedoja et al. 2011). Furthermore, the eastern region of the GSJB, mainly in the Pampa del Castillo area, has undergone widespread post-Miocene tectonic uplift

(Pedoja et al. 2011, Guillaume et al. 2013, Ávila and Dávila 2020). Pánek et al. (2025) suggested that the structuring of the Pampa del Castillo could be facilitated by gravitational processes, including lateral spreading and block slides, which affect Cenozoic rocks within a horst-and-graben topography during the Quaternary. Although in the San Bernardo fold belt, Quaternary mesoscopic reverse faults associated with compressional tectonics have been recognized (Gianni et al. 2017, Foix and Ocampo 2019, Ruiz 2024), the data from this study provide evidence of SSDS in the north flank of the GSJB, which is consistent with short-lived deformation events possibly related to seismic shaking under an extensional tectonic regime.

The tectonic complexity is further underscored by the coexistence of compressive tectonics along the San Bernardo fold belt and extensional processes in the eastern region of the GSJB, which is recorded from the Upper Cretaceous to the Middle Miocene (Giacosa et al. 2004, Ramos 2015, Allard et al. 2025). In this framework, the SSDS documented here may represent a younger expression of deformation in the eastern region of the basin, although the available data do not allow direct assignment to a specific seismogenic source.

The data obtained in this study were collected from horizontal (non-tilted) strata. Although local gravitational instabilities cannot be completely ruled out, the absence of regional tilting, together with the lateral continuity and stratigraphic recurrence observed particularly in event 2, does not support a purely gravitational origin for all deformed intervals, unlike those recognized by Pánek et al. (2025) for Cenozoic rocks structured during the Quaternary. This interpretation is also supported by the occurrence of discrete deformed horizons bounded by undeformed strata and by their association with synsedimentary normal faults. Historically, the uplift of extra-Andean Patagonia has been associated with the melting of the Llanquihue ice sheet (late Pleistocene), the regional equivalent of the Last Glacial Maximum (Rabassa and Clapperton 1990). However, models and calculations of isostatic rebound associated with glacial load cannot fully explain the uplift of extra-Andean Patagonia during the Quaternary (Ivins and James 2004, Klemann et al. 2007, Rostami et al. 2000, Pedoja et al. 2011). Alternatively, the uplift of extra-Andean Patagonia during the Quaternary has been interpreted as resulting from dynamic topography, based on the interaction of the Chilean Dorsal with the subduction zone and the generation of a slab window and slab tear, which allowed the ascent of the asthenosphere, the reorganization of mantle flow, and lithospheric thinning (Ávila and Dávila 2020, Navarrete et al. 2020, Ding et al. 2023, Navarrete 2025). In this context, the studied SSDS are consistent with episodic Quaternary deformation in the north flank of the GSJB. Although local autogenic processes may have contributed to some structures, the most laterally persistent and structurally organized intervals, particularly event 2, may reflect short-lived allogenic deformation possibly linked to seismic activity within the broader neotectonic evolution of extra-Andean Patagonia. However, additional chronological and paleoseismological constraints are required to better define the timing, recurrence, source, and magnitude of the inferred deformation events. Our research provides a foundation for future chronostratigraphic studies aimed at better constraining the ages of deformation events identified within the analyzed succession.

CONCLUSIONS

Soft-sediment deformation structures identified in Quaternary deposits of the north flank of the Golfo San Jorge Basin include brittle, fluid-escape, and ductile-deformation features. The deposits are contained within a 12.9 to 13.5 m-thick succession, composed of a lower coastal-marine unit, a middle fluvial unit, and an upper coastal-marine unit exposed along approximately 10 km of coastal cliffs. The main conclusions of the research are:

1) A total of 176 mesoscopic synsedimentary faults were identified, with 171 exhibiting normal kinematics (97.2%) and five faults exhibiting reverse kinematics (2.8%). The normal faults display strike directions ranging from NW-SE to NE-SW (average N 349°) and dip angles between 38° and 88° (average 60°). Exposed fault-plane lengths range from 0.78 to 134 cm, with a maximum vertical displacement of 21.4 cm. Damage zones contain secondary faults, joints, drag folds (monoclinal, anticlinal, and synclinal), and fault-propagation monoclines. Core zones are primarily composed of claystones, with minor amounts of calcium carbonate. Rake measurements on slickensides of the fault planes are approximately 90°.

2) The fluid-escape structures observed include pillars and convolute laminations, while ductile deformation structures consist of box-folds and recumbent folds. These features are consistent with deformation in water-saturated sediments after liquefaction and fluidization. However, their occurrence alone is not considered diagnostic of seismic shaking, because similar structures may also form through autogenic processes within coastal-marine depositional systems.

3) The deformed intervals show variable degrees of evidence for autogenic and allogenic triggering. Events 1, 2, and 4 include mesoscopic synsedimentary normal faults, although event 1 is locally preserved and has limited regional significance. Event 2 provides the strongest evidence for

short-lived allogenic deformation, possibly seismic shaking under an extensional tectonic regime, based on its occurrence in both studied localities, high abundance and diversity of SSDS, lateral persistence, correlation over ~10 km, and confinement within a discrete stratigraphic horizon bounded by undeformed strata. Nevertheless, some SSDS within event 2 may have been influenced or locally generated by autogenic processes, including tidal-channel margin instability, sedimentary loading, and pore-pressure fluctuations. Event 3 lacks synsedimentary normal faults and may record a stronger autogenic component. Event 4 records synsedimentary brittle deformation compatible with extensional tectonic activity, together with isolated fluid-escape structures that may reflect local autogenic processes; however, it is not interpreted here as a seismite sensu stricto.

4) Overall, the findings may be consistent with the persistence of extensional tectonic conditions in the eastern region of the Golfo San Jorge Basin during the Quaternary. In contrast, the San Bernardo fold belt and the western region underwent compressional tectonics. However, additional chronological and paleoseismological constraints are needed to confirm the timing, source, recurrence, and magnitude of the inferred deformation events.

ACKNOWLEDGEMENTS

The authors would like to thank the Department of Geology of the National University of Patagonia San Juan Bosco (UNPSJB) for providing the logistics for the fieldwork. Oporto Romero benefits from a grant from the Consejo Nacional de Investigaciones Científicas y Técnicas (CONICET) to develop his doctoral thesis. This paper is a contribution to the PI CIUNPAT 1966 (UNPSJB). The authors would like to thank the anonymous reviewers for their thorough and detailed evaluations. We are also grateful to Dr. Ricardo A. Astini, Editor-in-Chief of the journal, and Dr. Maisa A. Tunik, Associate Editor, for their valuable comments and critical observations during the review process, which further contributed to strengthening the manuscript.

REFERENCES

Aguirre, M.L. 2003. Late Pleistocene and Holocene palaeoenvironments in Golfo San Jorge, Patagonia: molluscan evidence. Marine Geology 194: 3–30.

Allard, J.O., Foix, N., Paredes, J.M., Giacosa, R.E., Bueti, S.A., Oporto Romero, F.E., and Rodriguez, R.A. 2025. Structural framework and evolution of the Golfo San Jorge Basin: a synthesis. Latin American Journal of Sedimentology and Basin Analysis 32(1): 19-31.

Allen, J.R.L. 1982. Sedimentary Structures – Their Character and Physical Basis, vol. II. Elsevier, 663 p. Amsterdam.

Allen, J.R.L., and Banks, N.L., 1972. An interpretation and analysis of recumbent-folded deformed cross-bedding. Sedimentology 19(3-4): 257-283.

Allen, J.R.L. 1977. The possible mechanics of convolute lamination in graded sand beds. Journal of the Geological Society of London 134: 19-31.

Ávila, P., and Dávila, F.M. 2020. Lithospheric thinning and dynamic uplift effects during slab window formation, southern Patagonia (45°-55° S). Journal of Geodynamics 133: 101689.

Bates, R.L., and Jackson, J.A. 1980. Glossary of Geology, 2nd Edition. American Geological Institute, 751 p., Falls Church, Virginia.

Becker, A. 1993. An attempt to define a “neotectonic period” for central and northern Europe. Geologische Rundschau 82: 67-83.

Bellosi, E.S. 1995. Paleogeografía y cambios ambientales de la Patagonia Central durante el Terciario Medio. Boletín de Informaciones Petroleras 44: 50-83. Buenos Aires.

Bezerra, F.H., and Vita-Finzi, C. 2000. How active is a passive margin? Paleoseismicity in northeastern Brazil. Geology 28(7): 591-594.

Bezerra, F.H., da Fonseca, V.P., Vita-Finzi, C., Lima-Filho, F.P., and Saadi, A. 2005. Liquefaction-induced structures in Quaternary alluvial gravels and gravelly sediments, NE Brazil. Engineering Geology 76(3-4): 191-208.

Bilmes, A., Cuitiño, J.I., and D’Elía, L. 2021. Los depósitos miocenos de Chubut: Análisis tectono-estratigráfico desde los Andes hasta el océano Atlántico. In: Giacosa, R.E. (Ed.), Geología y Recursos Naturales de la Provincia de Chubut. XXI Congreso Geológico Argentino, Relatorio: 1315-1334, Puerto Madryn.

Bryant, G., Cushman, R., Nick, K., and Miall, A. 2016. Paleohydrologic controls on soft-sediment deformation in the Navajo Sandstone. Sedimentary Geology 344: 205-221.

Bryant, G., Monegato, G., and Miall, A. 2013. An example of liquefaction-induced interdune sedimentation from the early Jurassic Navajo Sandstone, USA. Sedimentary Geology 297: 50-62.

Buchner, E., Sach, V.J., and Schmieder, M. 2020. New discovery of two seismite horizons challenges the Ries–Steinheim double-impact theory. Scientific Reports 10(1): 22143.

Childs, C., Nicol, A., Walsh, J.J., and Watterson, J. 2003. The growth and propagation of synsedimentary faults. Journal of Structural Geology 25(4): 633-648.

Childs, C., Holdsworth, R.E., Jackson, C.A.L., Manzocchi, T., Walsh, J.J., and Yielding, G. 2017. Introduction to the geometry and growth of normal faults. Geological Society of London, Special Publications 439: 1-9.

Codignotto, J.O., Kokot, R.R., and Marcomini, S.C. 1992. Neotectonism and sea-level changes in the coastal zone of Argentina. Journal of Coastal Research 8: 125–133.

Collinson, J.D., Mountney, N.P., and Thompson, D.B. 2006. Sedimentary Structures, 3rd ed. Terra Publishing, 292 p., Harpenden, England.

Conneally, J., Childs, C., and Nicol, A. 2017. Monocline formation during growth of segmented faults in the Taranaki Basin, offshore New Zealand. Tectonophysics 721: 310-321.

Cuitiño, J.I., Scasso, R., Ventura Santos, R., and Mancini, L. 2015. Sr ages for the Chenque Formation in the Comodoro Rivadavia region (Golfo San Jorge basin, Argentina): stratigraphic implications. Latin American Journal of Sedimentology and Basin Analysis 22(1): 3-12.

Delvaux, D., and Hanon, M. 1993. Neotectonics of the Mbeya area, SW Tanzania. Royal Museum for Central Africa, Annual Reports 1991–1992: 87–97. Tervuren, Belgium.

Desiage, P.A., St-Onge, G., Duchesne, M. J., Montero-Serrano, J.C., and Haller, M.J. 2023. Late Pleistocene and Holocene transgression inferred from the sediments of the Gulf of San Jorge, central Patagonia, Argentina. Journal of Quaternary Science 38(5): 629-646.

Ding, X., Dávila, F.M., and Lithgow-Bertelloni, C. 2023. Mechanisms of subsidence and uplift of Southern Patagonia and offshore basins during slab window formation. Geochemistry, Geophysics, Geosystems 24(5): e2022GC010844.

Djomeni, A.L., Ntamak-Nida, M.J., Mvondo Owono, F., Fowe Kwetche, P.G., Iboum Kissaaka, J.B., and Mooh-Enougui, E. 2011. Soft-sediment deformation structures in Mid-Cretaceous to Mid-Tertiary deposits, Centre East of the Douala sub-basin, Cameroon: preliminary results of the tectonic control. Syllabus Review 2(3): 92-105.

Doe, T.W., and Dott, R.H. 1980. Genetic significance of deformed cross bedding; with examples from the Navajo and Weber sandstones of Utah. Journal of Sedimentary Research 50(3): 793-812.

Elías, L., Montero-Lopez, C., Garcia, V.H., Escalante, L., Carabanti, D., and Bracco Boksar, R. 2022. Estructuras de deformación en sedimento blando como indicadoras de actividad tectónica cuaternaria en el sector austral del valle de Lerma, Noroeste Argentino. Revista de la Asociación Geológica Argentina 79(3): 516-535.

Encinas, A., Folguera, A., Bechis, F., Finger, K. L., Zambrano, P., Pérez, F., Bernabé, P., Tapia, F., Riffo, R., Buatois, L., Orts, D., Nielsen, S. N., Valencia, V., Cuitiño, J., Oliveros, V., De Girolamo Del Mauro, L., and Ramos, V. 2018. The late Oligocene-early Miocene marine transgression of Patagonia. In: Folguera, A., Contreras Reyes, E., Heredia, N., Encinas, A., Iannelli, S., Oliveros, V., Dávila, F., Collo, G., Giambiagi, L., Maksymowicz, A., Iglesia Llanos, M.P., Turienzo, M., Naipauer, M., Orts, D., Litvak, V., Alvarez, O., and Arriagada, C. (eds.). The Evolution of the Chilean-Argentinean Andes. Springer Earth System Sciences, Springer: 443-474, Cham.

Enzel, Y., Kadan, G., and Eyal, Y. 2000. Holocene earthquakes inferred from a fan-delta sequence in the Dead Sea graben. Quaternary Research 53(1): 34-48.

Ezpeleta, M., Ávila, P., Martina, F., Walz, I.T.K., Clutier, A., Rodríguez, M., Dagert, J.M., and Dávila, F.M. 2024. Tectonic and geodynamic controls on Oligocene–Miocene paleogeography and basin subsidence in southern Patagonia. Journal of South American Earth Sciences 136: 104800.

Faulkner, D.R., Jackson, C.A.L., Lunn, R.J., Schlische, R.W., Shipton, Z.K., Wibberley, C.A.J., and Withjack, M.O. 2010. A review of recent developments concerning the structure, mechanics and fluid flow properties of fault zones. Journal of Structural Geology 32(11): 1557-1575.

Feruglio, E. 1930. Observaciones acerca de un trabajo del Ing. T. Serghiescu sobre la región petrolífera de Comodoro Rivadavia. Boletín de Informaciones Petroleras 7(73): 833-862.

Feruglio, E. 1949. Descripción geológica de la Patagonia, vol. II. Yacimientos Petrolíferos Fiscales, 349 p., Buenos Aires.

Figari, E.G., Cid de la Paz, M.S., and Laffitte, G. 1996. Neocomian half graben in the western San Jorge Basin, Argentina: petroleum systems, origin and tectonic inversion. American Association of Petroleum Geologists Bulletin 80: 1289-1290.

Figari, E., Stelkov, E.E., Laffitte, G., Cid de la Paz, M., Courtade, S., Celaya, J., Vottero, A., Lafourcade, P., Martinez, R., and Villar, H. 1999. Los sistemas petroleros de la Cuenca del Golfo San Jorge: síntesis estructural, estratigráfica y geoquímica. 4° Congreso de Exploración y Desarrollo de Hidrocarburos, Actas: 197-237, Buenos Aires.

Figari, E.G., Scasso, R.A., Cúneo, R.N., and Escapa, I. 2015. Estratigrafía y evolución geológica de la Cuenca de Cañadón Asfalto, Provincia del Chubut, Argentina. Latin American Journal of Sedimentology and Basin Analysis 22(2): 135-169.

Fitzgerald, M.G., Mitchum, R.M., Uliana, M.A., and Biddle, K.T. 1990. Evolution of the San Jorge Basin, Argentina. American Association of Petroleum Geologists Bulletin 74 (6): 879-920.

Fossa-Mancini, E. 1931. Fallas y petróleo en la antigua Zona de Reserva Fiscal de 5.000 hectáreas de Comodoro Rivadavia. Boletín de Informaciones Petroleras 8(84): 539-560.

Fossa-Mancini, E. 1932. Faults in Comodoro Rivadavia oilfield, Argentina. American Association of Petroleum Geologists Bulletin 16(6): 556-576.

Fossa-Mancini, E. 1935. Las fallas de Comodoro Rivadavia en los estratos petrolíferos y en los afloramientos. Boletín de Informaciones Petroleras 12(136): 65-95.

Fossen, H. 2010. Structural Geology. Cambridge University Press, 457 p., Cambridge.

Foix, N., Paredes, J.M., and Giacosa, R.E. 2008. Paleo-earthquakes in passive-margin settings, an example from the Paleocene of the Golfo de San Jorge Basin, Argentina. Sedimentary Geology 205: 67-78.

Foix, N., Paredes, J.M., and Giacosa, R.E. 2012. Upper Cretaceous-Paleocene extensional phase in the Golfo San Jorge basin (Argentina): Growth-fault model, paleoseismicity and paleostress analysis. Journal of South American Earth Sciences 33: 110-118.

Foix, N., and Ocampo, S.M. 2019. Nuevas evidencias de neotectónica en la Faja Plegada San Bernardo, Cuenca del Golfo San Jorge, Chubut, Argentina. In: De Sosa Tomas, A., and Casal, G. (eds.), VII Jornadas

de las Ciencias de la Tierra “Dr. Eduardo Musacchio”, Resúmenes: 16-17, Comodoro Rivadavia.

Foix, N., Ocampo, S.M., Oporto Romero, F.E., Juárez, L., Rodríguez, S.S., Vidal, P.Á., and Iturra, D.A. 2022. Nuevas evidencias de tectónica extensional paleógena en el Flanco Norte de la cuenca del Golfo San Jorge, Estancia el Sol-Cañadón Hondo (Chubut, Argentina): resultados preliminares. In: Álvarez, B.N., and Farías Fuenzalida, L. (eds.), X Jornadas de las Ciencias de la Tierra “Dr. Eduardo Musacchio”, Resúmenes: 42-43, Comodoro Rivadavia.

Foix, N., Paredes, J.M., Oporto Romero, F.E., and Allard, J.O. 2025. Cenozoic stratigraphy of the Golfo San Jorge Basin, Argentina: an integrated record of tectonic, climatic, and eustatic control on basin evolution. Latin American Journal of Sedimentology and Basin Analysis 32(1): 68-80.

Genge, M. C., Zattin, M., Witt, C., Derycke, A., Gautheron, C., Mazzoli, S., Petrelli, M., Congé, N., Bosch, D., Bruguier, O., and Marquez, M. 2022. Denudation of the Cordillera and intraplate belt in Central Patagonia inferred by detrital multi-dating of foreland basin deposits. Sedimentary Geology 440: 106237.

Giacosa, R.E., Paredes, J.M., Nilini, A., Ledesma, M., and Colombo, F. 2004. Fallas normales de alto ángulo en el Neógeno del margen Atlántico de la Cuenca del Golfo San Jorge (46°S-67° 30′O, Patagonia Argentina). Boletín Geológico y Minero 115(3): 537-550.

Giacosa, R., Zubia, M., Sánchez, M., and Allard, J. 2010. Meso-Cenozoic tectonics of the southern Patagonian foreland: Structural evolution and implications for Au–Ag veins in the eastern Deseado Region (Santa Cruz, Argentina). Journal of South American Earth Sciences, 30(3-4): 134-150.

Gianni, G., Echaurren, A., Folguera, A., Likerman, J., Encinas, A., García, H.P.A., Dal Molin, C., and Valencia, V.A. 2017. Cenozoic intraplate tectonics in Central Patagonia: record of main Andean phases in a weak upper plate. Tectonophysics 721: 155-166.

Ginsberg, S.S. and Perillo, G.M.E. 1990. Channel bank recession in the Bahía Blanca estuary, Argentina. Journal of Coastal Research 6(4): 999-1009.

Guillaume, B., Martinod, J., Husson, L., Roddaz, M., and Riquelme, R. 2009. Neogene uplift of central eastern Patagonia: dynamic response to active spreading ridge subduction? Tectonics 28: 1-19.

Guillaume, B., Gautheron, C., Simon-Labric, T., Martinod, J., Roddaz, M., and Douville, E. 2013. Dynamic topography control on Patagonian relief evolution as inferred from low temperature thermochronology. Earth and Planetary Science Letters 364: 157-167.

Hancock, P.L. 1988. Neotectonics. Geology Ttoday 4(2): 57-61.

Horváth, Z., Michéli, E., Mindszenty, A., and Berényi-Üveges, J. 2005. Soft-sediment deformation structures in Late Miocene–Pleistocene sediments on the pediment of the Mátra Hills (Visonta, Atkár, Verseg): cryoturbation, load structures or seismites? Tectonophysics 410: 81–95.

Ivins, E.R., and James, T.S. 2004. Bedrock response to Llanquihue Holocene and present-day glaciation in southernmost South America. Geophysical Research Letters 31(24): 1-4.

Japas, M.S., Cortés, J.M., and Pasini, M. 2008. Tectónica extensional triásica en el sector norte de la cuenca Cuyana: primeros datos cinemáticos. Revista de la Asociación Geológica Argentina 63(2): 213-222.

Kim, Y.S., Peacock, D.C.P., and Sanderson, D.J. 2004. Fault damage zones. Journal of Structural Geology 26: 503-517.

Klemann, V., Ivins, E.R., Martinec, Z.K., and Wolf, D. 2007. Models of active glacial isostasy roofing warm subduction: case of the South Patagonian Ice Field. Journal of Geophysical Research 112: B09405.

Kunii, D., and Levenspiel, O. 1969. Fluidization Engineering. Wiley, New York, p. 534.

Legarreta, L., and Uliana, M. 1994. Asociaciones de fósiles y hiatos en el Supracretácico-Neógeno de Patagonia: una perspectiva estratigráfico-secuencial. Ameghiniana 31(3): 257-281.

Legarreta, L., Uliana, M., and Torres, M. 1990. Secuencias deposicionales cenozoicas de Patagonia Central: sus relaciones con las asociaciones de mamíferos terrestres y episodios marinos epicontinentales. 3º Simposio del Terciario de Chile, Actas: 135-176, Concepción.

Leidhold, C. 1934. La tectónica del subsuelo del campamento central de Comodoro Rivadavia. Boletín de Informaciones Petroleras 113: 71-77.

Le Heron, D.P., and Etienne, J.L. 2005. A complex subglacial clastic dyke swarm, Sólheimajökull, southern Iceland. Sedimentary Geology 181: 25–37.

Lowe, D.R. 1975. Water escape structures in coarse-grained sediments. Sedimentology 22: 157–204.

Lowe, D.R., and LoPiccolo, R.D. 1974. The characteristics and origins of dish and pillar structures. Journal of Sedimentary Petrology 44: 484–501.

Malumián, N., Ardolino, A.A., Franchi, M., Remesal, M., and Salani, F. 1999. La sedimentación y el volcanismo terciarios en la Patagonia extraandina. In: Caminos, R. (ed.), Geología Argentina. Instituto de Geología y Recursos Minerales, SEGEMAR, Anales 29(18): 557-612, Buenos Aires.

Martínez, O.A., and Kutschker, A. 2011. The “Rodados Patagónicos” (Patagonian shingle Formation) of eastern Patagonia: environmental conditions of gravel sedimentation. Biological Journal of the Linnean Society 103: 336-345.

Montenat, C., Barrier, P., Ott d’Estevou, P., and Hibsch, C. 2007. Seismites: An attempt at critical analysis and classification. Sedimentary Geology 196: 5-30.

Montes, A., Rodríguez, S.S., San Martín, C., and Allard, J.O. 2015. Migración de campos de dunas en cañadones costeros de Patagonia. Geomorfología e implicaciones paleoclimáticas. Revista de la Sociedad Geológica de España 28: 65-76.

Mohindra, R., and Bagati, T.N. 1996. Seismically induced soft-sediment deformation structures (seismites) around Sumdo in the lower Spiti valley (Tethys Himalaya). Sedimentary Geology 101(1-2): 69-83.

Moretti, M., and Sabato, L. 2007. Recognition of trigger mechanisms for soft-sediment deformation in the Pleistocene lacustrine deposits of the Sant'Arcangelo Basin (Southern Italy): seismic shock vs. overloading. Sedimentary Geology 196: 31-45.

Mountney, N.P. 2006. Eolian facies models. In: Posamentier, H.W., Walker, R.G. (Eds.), Facies Models Revisited. SEPM Special Publication 84: 19-83.

Nataraja, M.S., and Gill, H.S. 1983. Ocean wave-induced liquefaction analysis. Journal of Geotechnical Engineering 109: 573–590.

Navarrete, C.R. 2025. An overview of the Late Triassic–Pleistocene magmatism in the Golfo San Jorge Basin. Latin American Journal of Sedimentology and Basin Analysis 32(1): 6-18.

Navarrete, C.R., Gianni, G.M., and Folguera, A. 2015. Tectonic inversion events in the western San Jorge Gulf Basin from seismic, borehole and field data. Journal of South American Earth Sciences 64: 486-497.

Navarrete, C., Gianni, G., Massaferro, G., and Butler, K. 2020. The fate of the Farallon slab beneath Patagonia and its links to Cenozoic intraplate magmatism, marine transgressions and topographic uplift. Earth-Science Reviews 210: 103379.

Obermeier, S.F. 1996. Use of liquefaction-induced features for paleoseismic analysis – an overview of how seismic liquefaction features can be distinguished from other features and how their distribution and properties of source sediment can be used to infer the location and strength of Holocene paleo-earthquakes. Engineering Geology 44: 1–76.

Obruchev, V.A. 1948. Main features of kinetics and plastics of neotectonics. Izvestiya, Academy of Sciences USSR, Series: Geology, 5: 13–24.

Oporto Romero, F.E., and Paredes, J.M. 2022. Arquitectura estratigráfica de sistemas eólicos-fluviales: un ejemplo de la Formación Santa Cruz (Mioceno medio) en la cuenca del Golfo San Jorge, Argentina. Revista de la Asociación Geológica Argentina 79(1): 1-29.

Oporto Romero, F.E., Paredes, J.M., Allard, J.O., Foix, N., Valle, M.N., Cortés, M., Rodríguez, A.R., and Bueti, S.A. 2023. Arquitectura y análisis cinemático de fallas normales mesoscópicas: Formación Chenque (Mioceno Inferior-Medio) en el Sector Oriental de la cuenca del Golfo San Jorge, Patagonia central. Revista de la Asociación Geológica Argentina 80(3): 511-530.

Oporto Romero, F.E., Paredes, J.M., Allard, J.O., Perez Frasette, M.J., and Almada Báez, N. 2024a. Tectónica extensional en la sucesión continental miocena del Flanco Norte (cuenca del Golfo San Jorge): estructuras de deformación frágil, dúctil y de escape de fluidos. In: De Sosa Tomás, A., Díaz, R., and Farías Fuenzalida, L. (eds.), XI Jornadas de las Ciencias de la Tierra “Dr. Eduardo Musacchio”, Resúmenes: 63-64, Comodoro Rivadavia.

Oporto Romero, F.E., Paredes, J.M., Allard, J.O., and Turra, J.M. 2024b. Ciclicidad estratigráfica de sistemas fluviales-eólicos de la Formación Escalante (Mioceno Medio), Región Oriental de la cuenca del Golfo San Jorge. XXII Congreso Geológico Argentino, Resúmenes: 129-130, San Luis.

Owen, G. 1987. Deformation processes in unconsolidated sands. In: Jones, M.E., Preston, R.M.F. (Eds.), Deformation of Sediments and Sedimentary Rocks. Geological Society Special Publication 29: 11–24.

Owen, G. 2003. Load structures: gravity-driven sediment mobilization in the shallow subsurface. Geological Society Special Publications 216(1): 21–34.

Owen, G., and Moretti, M. 2011. Identifying triggers for liquefaction-induced soft-sediment deformation in sands. Sedimentary Geology 235 (3-4): 141-147.

Pánek, T., Břežný, M., Koláčková, B., Kilnar, J., and Winocur, D. 2025. Large lateral spreading and transient uplift of gravitational grabens along the passive continental margin (Pampa de Salamanca, Argentine Patagonia). Geomorphology 488: 109946.

Paredes, J.M., Foix, N., Guerstein, G.R., Guler, M.V., Irigoyen, M., Moscoso, P., and Giordano, S. 2015. A late Eocene-early Oligocene transgressive event in the Golfo San Jorge basin: palynological results and stratigraphic implications. Journal of South American Earth Sciences 63: 293-309.

Paredes, J.M., Foix, N., and Allard, J.O. 2021. Estratigrafía cretácica de la cuenca del Golfo San Jorge. In: Giacosa, R.E. (ed.), Geología y Recursos Naturales de la Provincia de Chubut. XXI Congreso Geológico Argentino, Relatorio: 142-186, Puerto Madryn, Argentina.

Pedoja, K., Regard, V., Husson, L., Martinod, J., Guillaume, B., Fucks, E., Iglesias, M., and Weill, P. 2011. Uplift of quaternary shorelines in eastern Patagonia: Darwin revisited. Geomorphology 127: 121-142.

Pinto, J.A., and Warme, J.E. 2016. Seismite in the Devonian Sultan Formation, Frenchman Mountain, Nevada: Evidence of far-field effect of the Alamo Event. The Mountain Geologist 53(2): 93-114.

Plazibat, S., Rasgido, A., and Paredes, J.M. 2019. Subsurface characterization of Cenozoic igneous activity at Cerro Dragón area (Golfo San Jorge Basin, central Patagonia): Implications for basin evolution and hydrocarbon prospectivity. Journal of South American Earth Sciences 96: 102389.

Postma, G. 1983. Water escape structures in the context of a depositional model of a mass flow dominated conglomeratic fan-delta (Abrioja Formation, Pliocene, Almeria Basin, SE Spain). Sedimentology 30: 91–103.

Rabassa, J., and Clapperton, C.M. 1990. Quaternary glaciations of the southern Andes. Quaternary Science Reviews 9(2-3): 153-174.

Raigemborn, M.S., Krause, J.M., Bellosi, E.S., and Matheos, S.D. 2010. Redefinición estratigráfica del Grupo Río Chico (Paleógeno Superior), en el norte de la cuenca del Golfo San Jorge, Chubut. Revista de la Asociación Geológica Argentina 67: 239-256.

Ramos, V.A. 2015. Evolución de la Cuenca Golfo San Jorge: su estructuración y régimen tectónico. Revista de la Asociación Geológica Argentina 72(1): 12-20.

Rijsdijk, K.F., Owen, G., Warren, W.P., McCarroll, D., and van der Meer, J.J.M. 1999. Clastic dykes in over-consolidated tills: evidence for sub-

glacial hydrofracturing at Killiney Bay, eastern Ireland. Sedimentary Geology 129: 111-126.

Rodríguez, J.F.R., and Littke, R. 2001. Petroleum generation and accumulation in the Golfo San Jorge basin, Argentina: a basin modeling study. Marine and Petroleum Geology 18(9): 995-1028.

Rodríguez, S.S., Montes, A., Villarosa, G., Outes, V., and Ruiz, P.M. 2025. Dispersión y preservación de tefras en la Patagonia extraandina, asociadas a la erupción H2 del volcán Hudson, durante el Holoceno tardío. Revista de la Asociación Geológica Argentina 82(1): 56-79.

Rostami, K., Peltier, W.R., and Mangini, A. 2000. Quaternary marine terraces, sea-level changes and uplift history of Patagonia, Argentina: comparisons with predictions of the ICE-4G (VM2) model of the global process of glacial isostatic adjustment. Quaternary Science Reviews 19: 1495-1525.

Rossetti, D.F. 1999. Soft-sediment deformation structures in late Albian to Cenomanian deposits, São Luís Basin, northern Brazil: evidence for palaeoseismicity. Sedimentology 46(6): 1065-1081.

Rossetti, D.F., Bezerra, F.H.R., Góes, A.M., and Neves, B.B. 2011. Sediment deformation in Miocene and post-Miocene strata, Northeastern Brazil: evidence for paleoseismicity in a passive margin. Sedimentary Geology 235(3-4): 172-187.

Ruiz, P.M. 2024. Geomorfología y evolución geológica del Bajo Slápeliz, Patagonia Argentina. Tesis de grado, Facultad de Ciencias Naturales y Ciencias de la Salud, Universidad Nacional de la Patagonia San Juan Bosco (inédita), 158 p., Comodoro Rivadavia.

Santos, M.G., and Henrique-Pinto, R. 2022. Multi-scale, multi-style soft-sediment deformation structures preserved in Cenozoic fluvial deposits, southeastern Brazil: Evidence of impact shaking?. Sedimentary Geology 442: 106279.

Scasso, R.A., Dozo, M.T., Cuitiño, J.I. and Bouza, P.J. 2012. Meandering tidal-fluvial channels and lag concentration of terrestrial vertebrates in the fluvial-tidal transition of an ancient estuary in Patagonia. Latin American Journal of Sedimentology and Basin Analysis 19(1): 27-45.

Schellmann, G., and Radtke, U. 1997. Electron spin resonance (ESR) techniques applied to mollusc shells from South America (Chile, Argentina) and implications for palaeo sea-level curve. Quaternary Science Reviews 16: 465-475.

Schellmann, G., and Radtke, U. 2000. ESR dating stratigraphically well-constrained marine terraces along the Patagonian Atlantic coast (Argentina). Quaternary International 68–71: 261-273.

Schellmann, G., and Radtke, U. 2003. Coastal terraces and Holocene sea-level changes along the Patagonian Atlantic coast. Journal of Coastal Research 19: 983–996.

Schellmann, G., and Radtke, U. 2010. Timing and magnitude of Holocene sea-level changes along the middle and south Patagonian Atlantic coast derived from beach ridge systems, littoral terraces and valley-mouth terraces. Earth-Science Reviews 103(1-2): 1-30.

Sciutto, J.C., César, O., Escribano, V., and Pezzuchi, H.D. 2000. Hoja Geológica 4566-III, Comodoro Rivadavia, provincia del Chubut. Instituto de Geología y Recursos Minerales. Servicio Geológico Minero Argentino, Boletín 244: 1-52.

Sciutto, J.C., César, O., and Iantanos, N. 2008. Hoja Geológica 4569-IV, Escalante, provincia del Chubut. Instituto de Geología y Recursos Minerales. Servicio Geológico Minero Argentino, Boletín 351: 1-76.

Seed, H.B., and Idriss, I.M. 1971. A simplified procedure for evaluating soil liquefaction potential. Journal of Soil Mechanics and Foundation Engineering 97 (9): 1249–1273.

Seilacher, A. 1969. Fault-graded beds interpreted as seismites. Sedimentology 13(1-2): 155-159.

Seth, A., Sarkar, S., and Bose, P.K. 1990. Synsedimentary seismic activity in an immature passive margin basin (Lower Member of the Katrol Formation, Upper Jurassic, Kutch, India). Sedimentary Geology 68(4): 279-291.

Shanmugam, G. 2016. The seismite problem. Journal of Palaeogeography 5(4): 318-362.

Sylwan, C.A. 2001. Geology of the Golfo San Jorge basin, Argentina. Journal of Iberian Geology 27: 123-157.

Thorsen, C.E. 1963. Age of growth faulting in southeast Louisiana. Transactions of the Gulf Coast Association of Geological Societies 13: 103-110.

Twiss, R.J., and Moores, E.M. 1992. Structural geology. W.H. Freeman, 532 p., New York.

Üner, S. 2014. Seismogenic structures in Quaternary lacustrine deposits of Lake Van (eastern Turkey). Geologos 20: 79–87.

Van Balen, R.T., Houtgast, R.F., and Cloetingh, S.A.P.L. 2005. Neotectonics of The Netherlands: a review. Quaternary Science Reviews 24(3-4): 439-454.

Van Vliet-Lanoë, B., Magyari, A., and Meilliez, F. 2004. Distinguishing between tectonic and periglacial deformations of quaternary continental deposits in Europe. Global and Planetary Change 43: 103–127.

Zhang, K., Wang, Y., Zhang, G., Xu, T., Xiong, W., Wang, S., Ma, J., and Sun, T. 2022. Discovery of Seismites in the Carboniferous Formation of the Shibei Sag (China) and Its Petroleum Geological Significance. Minerals 12(12): 1560.